



1 Changes of regional meteorology induced by anthropogenic heat 2 and their impacts on air quality in South China

3 Min Xie^{1,2*}, Kuanguang Zhu^{1,3}, Tijian Wang^{1,4*}, Wen Feng², Minggao Li³, Mengmeng Li¹, Yong
4 Han¹, Shu Li¹, Bingliang Zhuang¹, Lei Shu¹, Da Gao¹, Jingbiao Liao¹

5 ¹ School of Atmospheric Sciences, Nanjing University, Nanjing, China;

6 ² Key Laboratory of South China Sea Meteorological Disaster Prevention and Mitigation of
7 Hainan Province, Haikou, China

8 ³ Hubei Academy of Environmental Science, Wuhan, China

9 ⁴ CMA-NJU Joint Laboratory for Climate Prediction Studies, Institute for Climate and Global
10 Change Research, School of Atmospheric Sciences, Nanjing University, Nanjing, China

11

12 **Abstract:** Anthropogenic heat (AH) emissions from human activities can change the urban
13 circulation and thereby affect the air pollution in and around cities. Based on statistic data, the
14 spatial distribution of AH flux in South China is estimated. With the aid of the WRF/Chem model
15 in which the AH parameterization is developed to incorporate the gridded AH emissions with
16 temporal variation, the simulations for January and July in 2014 are performed over South China.
17 By analyzing the differences between the simulations with and without adding AH, the impact of
18 AH on regional meteorology and air quality are quantified. The results show that the regional
19 annual mean AH fluxes over South China are only 0.87W/m^2 , but the values for the urban areas of
20 the Pearl River Delta (PRD) region can be close to 60W/m^2 . These AH emissions can
21 significantly change the urban heat island and urban-breeze circulations in the big cities. In the
22 PRD city cluster, 2-m air temperature rises up by 1.1°C in January and over 0.5°C in July, the
23 boundary layer height increases by 120m in January and 90m in July, 10-m wind speed is
24 intensified over 0.35 m/s in January and 0.3 m/s in July, and the accumulative precipitation is
25 enhanced by 20-40% in July. These changes of meteorological conditions can significantly impact
26 the spatial and vertical distributions of air pollutants. Due to the increases of PBLH, surface wind
27 speed and upward vertical movement, the concentrations of primary air pollutants decrease near
28 surface and increase at the upper levels. But the vertical changes of O_3 concentrations show the
29 different patterns in different seasons. The surface O_3 concentrations in big cities increase with
30 maximum values over 2.5ppb in January, while O_3 is reduced at the lower layers and increases at
31 the upper layers above some megacities in July. This phenomenon should be attributed to the facts
32 that the chemical effects can play a significant role in O_3 changes over South China in winter,
33 while the vertical movement can be the dominant effect in some big cities in summer. Adding the
34 gridded AH emissions can better describe the heterogeneous impacts of AH on regional
35 meteorology and air quality, suggesting that more studies on AH should be carried out in the
36 climate and air quality assessments.

37 **Key words:** Anthropogenic heat; PRD; WRF/Chem; PM_{10} ; O_3



38

39

40 *Corresponding author, +86-25-89685302

41 E-mail address: minxie@nju.edu.cn, tjwang@nju.edu.cn

42

43 Urbanization and its impacts on regional meteorology and air quality have been widely
44 acknowledged, observed, and investigated (Rizwan et al., 2008; Mirzaei and Haghighat, 2010).
45 Previous studies have illustrated that urbanization can affect atmospheric environment in many
46 ways, which are mainly associated with the increase of air pollutant emissions from the
47 intensification of energy consumptions (Akbari et al., 2001; Civerolo et al., 2007; Jiang et al, 2008;
48 Stone, 2008; Chen et al., 2014b), the change of land covers from natural surfaces to artificial ones
49 (Civerolo et al., 2007; Lo et al., 2007; Wang et al., 2007; 2009b; Jiang et al., 2008; Zhang et al.,
50 2009; Lu et al., 2010; Wu et al., 2011; Chen et al., 2014b; Liao et al., 2015; Zhu et al., 2015; Li et
51 al., 2016), and the release of anthropogenic heat from human activities in cities (Ryu et al., 2013;
52 Yu et al., 2014; Xie et al., 2016). Anthropogenic heat (AH) can increase turbulent fluxes in
53 sensible and latent heat (Oke, 1988), implying that it can modulates local and regional
54 meteorological processes (Ichinose et al., 1999; Block et al., 2004; Fan and Sailor, 2005; Ferguson
55 and Woodbury, 2007; Chen et al., 2009; Zhu et al., 2010; Feng et al., 2012; 2014; Menberg et al.,
56 2013; Ryu et al., 2013; Wu and Yang, 2013; Bohnenstengel et al., 2014; Chen et al., 2014a; Meng
57 et al., 2011; Yu et al., 2014; Xie et al., 2016) and thereby exert an important influence on the
58 formation and the distribution of ozone (Ryu et al., 2013; Yu et al., 2014; Xie et al., 2016) as well
59 as aerosols (Yu et al., 2014; Xie et al., 2016).

60 Previous studies on AH basically focused on the amount of heat fluxes or their effects on
61 meteorology. It was reported that the typical values of AH fluxes in urban areas range from 20 to
62 100 W/m² (Crutzen, 2004; Sailor and Lu, 2004; Fan and Sailor, 2005; Pigeon et al., 2007; Lee et
63 al., 2009; Iamarino et al., 2012; Lu et al., 2016; Xie et al., 2016). Sometimes, the fluxes might
64 exceed the value of 100 W/m² (Iamarino et al., 2012; Quah and Roth, 2012; Lu et al., 2016; Xie et
65 al., 2016), with the extreme value of 1590 W/m² in the densest part of Tokyo at the peak of
66 air-conditioning demand (Ichinose et al., 1999). In regard to their effects, the researchers found
67 that AH fluxes can cause urban air temperatures to increase by several degrees (Fan and Sailor,
68 2005; Ferguson and Woodbury, 2007; Chen et al., 2009; Zhu et al., 2010; Feng et al., 2012; 2014;
69 Menberg et al., 2013; Wu and Yang, 2013; Bohnenstengel et al., 2014; Chen et al., 2014a; Yu et al.,
70 2014; Xie et al., 2016), induce the atmosphere more turbulent and unstable, change the urban heat
71 island circulation, strengthen the air vertical movement (Ichinose et al., 1999; Block et al., 2004;
72 Fan and Sailor, 2005; Chen et al., 2009; Feng et al., 2012; 2014; Bohnenstengel et al., 2014; Yu et
73 al., 2014; Xie et al., 2016), enhance the convergence of water vapor in cities, and change the
74 regional precipitation patterns (Feng et al., 2012; 2014; Xie et al., 2016). In spite that meteorology
75 conditions and air quality are inextricably linked, however, few investigations have paid attention



76 to how the air quality is altered by the changes of regional meteorology induced by anthropogenic
77 heat. The results from the limited studies have showed that this impact is significant in and around
78 large urban areas and should be considered in the air pollution predictions (Ryu et al., 2013; Yu et
79 al., 2014; Xie et al., 2016).

80 Over the past decades, many areas in South China have been suffering the air quality
81 deterioration (Wang et al., 2007; 2009b; Chan and Yao, 2008; Liu et al., 2013b), with high ozone
82 (O_3) or poor visibility frequently occurring in urban areas (Wang et al., 2007; Fang et al., 2009)
83 and the background air pollutant concentrations steadily increasing (Wang et al., 2009a; Liu et al.,
84 2013b). These air pollutions may be related with the rapid urban expansion. As the most urbanized
85 and industrialized part of South China, the Pearl River Delta (PRD) region has become the largest
86 metropolitan area in the world within a very short time (World Bank Group, 2015). Thus, many
87 previous studies have tried to figure out the effects of urbanization on urban climate and air quality
88 in this region (Lo et al., 2007; Wang et al., 2007; 2009b; Lu et al., 2010; Meng et al., 2011; Wu et
89 al., 2011; Zhang et al., 2011; Feng et al., 2012; 2014; Chen et al., 2014b; Li et al., 2014; 2016).
90 Among these studies, most researchers merely investigated how the expansion of urban land-use
91 influences the meteorology processes (Lo et al., 2007; Wang et al., 2007; 2009b; Lu et al., 2010;
92 Meng et al., 2011; Wu et al., 2011; Feng et al., 2012; Chen et al., 2014b; Li et al., 2016). Some also
93 linked these changes of meteorological factors with the regional air quality, and quantified the
94 impacts of land-use changing on air pollution (Wang et al., 2007; 2009b; Feng et al., 2012; Chen
95 et al., 2014b; Li et al., 2014; 2016). Only a few researchers took AH into account (Meng et al.,
96 2011; Feng et al., 2012; 2014). But they just clarified the impact of AH on meteorological
97 conditions by merely adopting the fixed AH value in the urban parameterization scheme of
98 meteorological models (Meng et al., 2011; Feng et al., 2012). Consequently, we still need to
99 further understand how the excessive anthropogenic heat from urban expansion impacts on the
100 severe air quality problems in this world famous region.

101 To fill the abovementioned knowledge gap, we present our new findings on the impact
102 mechanism of anthropogenic heat on urban climate and regional air quality over South China in
103 this paper, including (1) the spatial and temporal characteristics of AH emissions in South China,
104 (2) how to implement the inhomogeneous AH data into the air quality model WRF/Chem, (3) the
105 impacts of AH fluxes on meteorological fields, and (4) the impacts of meteorology changes on the
106 air quality in different cities over South China. Detailed descriptions about the estimating method
107 for anthropogenic heat emissions, the adopted WRF/Chem model with special configurations, and
108 the observation data for model validation are presented in Sect. 2. Main results, including the
109 inhomogeneous distribution of AH, the model evaluation, and the three-dimensional changes of
110 meteorological fields and air pollutant concentrations are presented in Sect. 3. The summary is
111 given in Sect. 4.

112

113 2. Methodology and data



114 2.1 Method for estimating anthropogenic heat fluxes

115 The top-down energy inventory method, which predicts AH emissions based on the statistics
 116 data of energy consumption, is the most common approach and widely used all over the world
 117 (Sailor and Lu, 2004; Flanner, 2009; Hamilton et al., 2009; Lee et al., 2009; Allen et al., 2011;
 118 Iamarino et al., 2012; Quah and Roth, 2012; Chen et al., 2014a) as well as in China (Chen et al.,
 119 2012; Xie et al., 2015; 2016; Lu et al., 2016). On basis of the previous studies, AH fluxes over the
 120 area between (101°E, 16°N) and (119°E, 26°N) in 1990, 1995, 2000, 2005, 2010 and 2014 are
 121 calculated in this study by the following equation:

$$122 \quad Q_F = Q_{FI} + Q_{FB} + Q_{FV} + Q_{FHM} \quad (1)$$

123 where, Q_F is the total anthropogenic heat flux (W/m^2); Q_{FI} , Q_{FB} , Q_{FV} , and Q_{FHM} represent the heat
 124 emitted from the industry sector, buildings, vehicles and human metabolism (W/m^2), respectively.
 125 To accurate estimate the spatial heterogeneity of AH fluxes, the estimated area is gridded as 456
 126 rows and 264 columns with the grid spacing of 2.5 arcmin. The heat flux generated by human
 127 metabolism at each grid is estimated as:

$$128 \quad Q_{FHM} = P \cdot (M_d \cdot h_d + M_n \cdot h_n) / h \quad (2)$$

129 where, P is the population number at a grid. h_d , h_n and h are the hours of daytime, nighttime and a
 130 whole day. In this study, they are set to be 16, 8 and 24, respectively. M_d and M_n are the average
 131 human metabolic rate (W/person) during the daytime and at night. Referring to the previous
 132 studies (Sailor and Lu, 2004; Chen et al., 2012; Quah and Roth, 2012; Xie et al., 2015; 2016; Lu et
 133 al., 2016), we determined that the metabolic rate of a typical man is 175 W for the active daytime
 134 (M_d) and 75 W for the sleep period (M_n).

135 Based on the work of Flanner (2009), Lu et al. (2016) and Xie et al. (2016), it is reasonably
 136 assumed that all non-renewable primary energy consumption used for human activities is
 137 thermally dissipated as AH. So, Q_{FI} , Q_{FB} , and Q_{FV} at each grid can be estimated by using the data
 138 of non-renewable energy consumption (coal, petroleum, natural gas, and electricity etc.) from
 139 different categories. The amount of AH fluxes for one category can be estimated by the following
 140 equation:

$$141 \quad Q_x = \eta \cdot \varepsilon \cdot C / (t \cdot A) \quad (3)$$

142 where, Q_x represents Q_{FI} , Q_{FB} or Q_{FV} . C is the primary energy consumption from a category at a
 143 grid (metric ton standard coal). ε is the calorific value of standard coal equivalent, with the
 144 recommended value of $29.271 \times 10^3 \text{ kJ/kg}$ (Chen et al., 2012; Lu et al., 2016; Xie et al., 2015;
 145 2016). η is the efficiency of heat release, with the typical value of 60% for electricity or
 146 heat-supply sector and 100% for other sectors (Lu et al., 2016; Xie et al., 2016). t is the time
 147 duration of used data, which is set to be 31536000 s (seconds in a year) in this study. A represents
 148 the area of a grid (km^2). To quantify the value of C for each grid, we first of all obtain the energy
 149 consumption data from 1990 to 2014 in China Energy Statistical Yearbooks. Then we double
 150 check and modify the data in typical cities on basis of the Yearbooks in Guangdong, Guangxi,
 151 Hainan province and Hong Kong. In the end, the total numbers are apportioned according to the



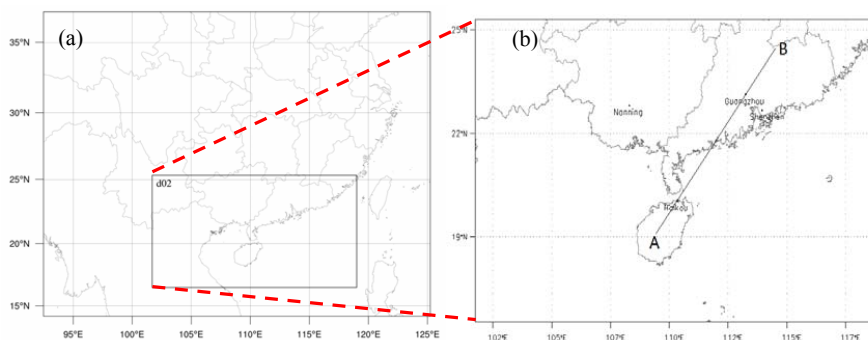
152 value of gross domestic product (GDP) or population density at each grid. GDP is used for
153 industry and vehicle, while population is chosen for building. The population density with the
154 resolution of 2.5 arcmin in 1990, 1995, 2000, 2005 and 2010 can be downloaded from Columbia
155 University's Socioeconomic Data and Applications Center. The gridded GDP data are developed
156 and applied based on the work of Liu et al. (2013a). The spatial distributions of GDP and
157 population in 2014 are unobtainable, and thereby the data in 2010 are used as the surrogates.

158 2.2 WRF/Chem and its configuration

159 The WRF/Chem version 3.5 is applied to investigate the impacts of AH fluxes on regional
160 meteorology and air quality over South China. WRF/Chem is a new generation of air quality
161 modeling system, in which the feedbacks between meteorology and air pollutants are included by
162 fully coupling the meteorological model (WRF) with the chemical modules (Chem). WRF/Chem
163 has been widely used in simulating air quality in China and proved to be a reliable modeling tool
164 from city-scale to meso-scale (Wang et al., 2009b; Liu et al., 2013; Yu et al., 2014; Liao et al.,
165 2015; Xie et al., 2016).

166 Three simulations are conducted in this study. One does not take the contribution of AH into
167 account while the other two incorporate WRF/Chem with the fixed or the inhomogeneous AH
168 fluxes (The details are presented in Sect. 2.3). Except for the setting of AH parameterization, other
169 configurations (such as the physical schemes, the chemical schemes and the emission inventories
170 etc.) for all simulations are the same. Thus, the difference between the modeling results can
171 illustrate the effects of AH. As shown in Fig. 1, two nested domains are used. The outermost
172 domain (Domain 1, D01) has the horizontal grids of 121×95 , with the grid resolution of $27\text{km} \times$
173 27km . The second domain (Domain 2, D02) covers Guangdong, Guangxi, and Hainan provinces,
174 with the center point at $(110.4^\circ\text{E}, 20.9^\circ\text{N})$, the horizontal grids of 192×105 , and the grid spacing
175 of 9km . For all domains, from the ground level to the top pressure of 100hPa , there are 31 vertical
176 sigma layers with about 10 in the planetary boundary layer (PBL). January and July in 2014 are
177 chosen for simulations and analysis. January and July are used to represent the hot and the cold
178 weather condition, respectively.

179



180

181 **Fig. 1. WRF/Chem domain configuration: (a) tow domains for simulations and (b) enlarged view of domain**



182 **2 with the cities in South China where the observation sites are located. Line AB in (b) denotes the location**
 183 **of the vertical cross section used in Fig. 4, Fig. 6, Fig. 8, Fig. 9, and Fig. 10.**

184

185 The detailed options for the physical and chemical parameterization schemes used in this
 186 study are shown in Table 1. Additionally, a Single Layer Urban Canopy Model (SLUCM) coupled
 187 in Noah Land Surface Model (Noah/LSM) is adopted for better modeling the urban effects.
 188 Following the work of Liu et al. (2013), the default values for urban canopy parameters in
 189 SLUCM are substituted by the typical values in South China. The recently updated Moderate
 190 Resolution Imaging Spectroradiometer (MODIS) land-use data (20 categories) with the resolution
 191 of 30-sec are used to replace the default USGS (U.S. Geological Survey) land-use data in
 192 WRF/Chem, because the USGS data are too outdated to illustrate the intensive urbanization over
 193 South China. For chemistry, the RADM2 gas-phase chemistry scheme and the MADE/SORGAM
 194 aerosol scheme are adopted. RADM2 (Regional Acid Deposition Model version 2) contains 63
 195 prognostic species and 136 reactions (Balzarini et al., 2015). MADE/SORGAM is the classical
 196 aerosol module used in WRF/Chem (Grell et al., 2005), where the Aerosol Dynamics Model for
 197 Europe (MADE) (Ackermann et al., 1998) contains the Secondary Organic Aerosol Model
 198 (SORGAM) (Schell et al., 2001). The anthropogenic emissions are mainly from the 2012-year
 199 Multi-resolution Emission Inventory for China (MEIC) with $0.25^\circ \times 0.25^\circ$ resolution. This MEIC
 200 inventory based on RADM2 mechanism is re-projected for the grids of China in both domains.
 201 For the grids outside of China, the inventory developed by Zhang et al. (2009) is used. The
 202 biomass burning emissions are acquired from the work of Li et al. (2016). The biogenic emissions
 203 are calculated online by using MEGAN2.04 (Guenther et al., 2006). The NCEP global reanalysis
 204 data with the spatial resolution of $1^\circ \times 1^\circ$ and 27 vertical levels are selected to provide the initial
 205 meteorological fields and boundary conditions. The initial chemical state and boundary conditions
 206 are obtained from the modeling results from the global chemistry transport model MOZART-4.

207

208 **Table 1. The grid settings, physics and chemistry options for all simulations**

Items	Contents
Dimensions (x,y)	(121,95), (192,105)
Grid size (km)	27, 9
Time step (s)	150
Microphysics	Purdue Lin microphysics scheme (Lin et al., 1983)
Long-wave radiation	RRTM scheme (Mlawer et al., 1997)
Short-wave radiation	Goddard scheme (Kim and Wang, 2011)
Cumulus parameterization	Grell 3D (Grell and Devenyi, 2002)
Surface layer	Eta similarity (Janjic, 1994)
Land surface	Noah land surface model (Chen and Dudhia, 2001)
Planetary boundary layer	Mellor-Yamada-Janjic scheme (Janjic, 1994)
Gas-phase chemistry	RADM2 (Stockwell et al., 1990)
Photolysis scheme	Madronich photolysis (Madronich, 1987)
Aerosol module	MADE (Ackermann et al., 1998) / SORGAM (Schell et al., 2001)

209

210 **2.3 The configurations for AH parameterization**

211 As shown in Table 2, three cases of numerical experiments are performed to evaluate the
 212 effects of AH. Non_AH is the base case, which does not consider the effects of AH. In Fix_AH,



213 the default option for AH in SLUCM of WRF/Chem is adopted. For Grd_AH, we modify the AH
214 parameterization, and the gridded AH flux data estimated in Sect. 2.1 are used to simulation the
215 spatial heterogeneous effects of AH on meteorology and air quality. The difference between the
216 modeling results of Fix_AH and Grd_AH can illustrate the model improvement caused by
217 considering the spatial heterogeneity of AH. Comparing the results from Non_AH and Grd_AH,
218 we can finally demonstrate the exact impacts of anthropogenic heat.

219

220 **Table 2. Three simulations conducted in this study**

Cases	Description
Non_AH	excluding anthropogenic heat emissions in SLUCM
Fix_AH	including anthropogenic heat emissions in SLUCM, but using the default AH option with fixed value 50 W/m ² for all urban grids
Grd_AH	including anthropogenic heat emissions in SLUCM, and using the inhomogeneous AH emissions in 2014 estimated in Sect. 2.1

221

222 In SLUCM of WRF/Chem, the AH for one grid is determined by the fixed AH value, the
223 fixed temporal diurnal pattern, and the urban fraction value (Chen et al., 2011; Yu et al., 2014; Xie
224 et al., 2016). This default parameterization for AH can be described by the following algorithm:

$$225 \quad SH = F_V \cdot SH_V + F_U \cdot (SH_U + AH_{fixed}) \quad (4)$$

226 where SH is the total sensible heat flux in a grid. F_V and SH_V are the fractional coverage and the
227 sensible heat flux of vegetations, respectively. F_U and SH_U are those of urban surfaces. AH_{fixed}
228 represents the fixed AH value for all urban areas (Chen et al., 2011). With respect to Grd_AH, we
229 modify Eq. 4 by incorporating the inhomogeneous AH data (Q_F) as follow:

$$230 \quad SH = F_V \cdot SH_V + F_U \cdot (SH_U + Q_F) \quad (5)$$

231 The gridded AH fluxes in 2014 from Sect. 2.1 (with the grid spacing of about 4km) are
232 re-projected to domain 2 (9km) by the coordinates of each grid. To account for temporal variability,
233 the diurnal variation pattern recommended for PRD by Zheng et al. (2009) and Lu et al. (2016) is
234 adopted. It was reported that there is no significant seasonal difference in heating over South
235 China (Lu et al., 2016). Thus, the monthly variation of AH is not considered in this study.

236 **2.4 Method for model evaluation**

237 The observation data of meteorology factors and air pollutants in Guangzhou, Shenzhen,
238 Nanning and Haikou are used to validate the WRF/Chem simulations in this study. The hourly
239 observation records of 2-m temperature, 10-m wind speed and 2-m relative humidity in January
240 and July of 2014 can be obtained from the National Meteorological center of China
241 Meteorological Administration. The relevant time series of PM₁₀ and O₃ concentrations can be
242 acquired from China National Environmental Monitoring Center. The assurance/quality control
243 (QA/QC) procedures for these data strictly follow the national standards. As described by Liao et
244 al. (2015) and Xie et al. (2016), the mean bias (MB), root mean square error (RMSE) and
245 correlation coefficient (COR) between observation records and modeling results are used to
246 evaluate the model performance.

247

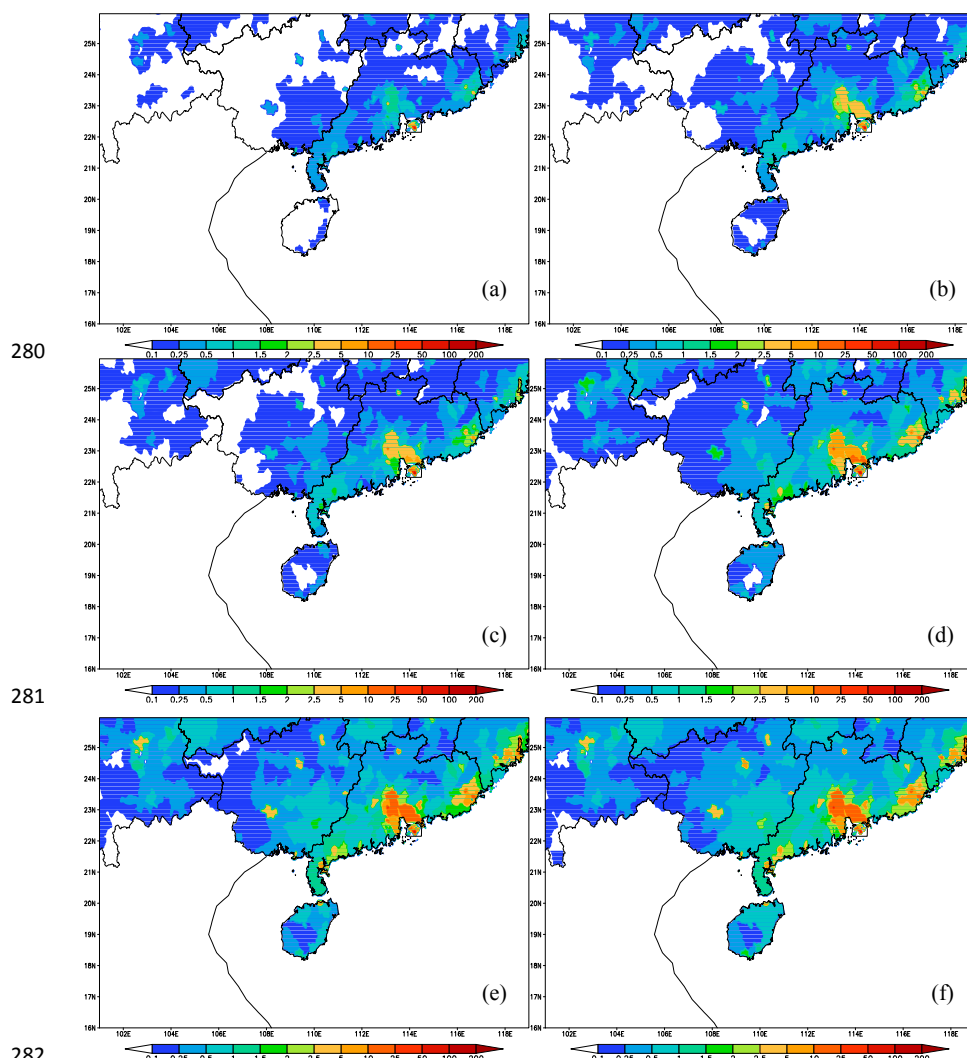


248 **3. Results and discussions**

249 **3.1 Spatial distribution of AH fluxes in South China**

250 Fig. 2 shows the spatial distribution of AH in 1990, 1995, 2000, 2005, 2010 and 2014 over
251 South China. Obviously, big cities especially the cities in PRD have the largest values from the
252 1990s till now. In 1990, except for those in Guangdong and Hong Kong, the AH fluxes in most
253 areas of South China are less than 2 W/m^2 . From 1995 to 2000, the AH fluxes in most parts of
254 PRD (except for those in Hong Kong) are less than 5 W/m^2 , and those in other areas of South
255 China are generally lower than 2.5 W/m^2 . After 2005, however, the AH fluxes exceed 10 W/m^2 in
256 many cities of South China, with the high values over 50 W/m^2 in and around Hong Kong. For the
257 annual mean AH flux over the whole administrative district of different province, the value in
258 Guangdong continuously increases from 0.30 W/m^2 for 1990 to 1.68 W/m^2 for 2014, while the
259 heat release in Guangxi and Hainan keeps in a low level ($< 0.5 \text{ W/m}^2$) but with an obvious
260 increasing. The annual mean AH values in the downtown areas are much higher than the regional
261 ones. For instance, the PRD city cluster always has the highest anthropogenic heat emissions in
262 South China. As shown in Table 3, the annual mean value in the built-up areas aggrandizes from
263 5.1 W/m^2 in 1990 to 58 W/m^2 in 2014. These results are similar to those reported by Chen et al.
264 (2012a; 2014) and Xie et al. (2015), and the temporal variation pattern also fits in well with the
265 economic boom over South China in the past decades.

266 In 2014, as illustrated in Fig. 4f, most important cities in South China have the AH fluxes
267 more than 5 W/m^2 . High fluxes generally occur in Guangdong province, especially in the PRD
268 region and the Chao-Shan area, with the typical values over 10 W/m^2 . In the build-up area of
269 Guangzhou, the AH fluxes are close to 60 W/m^2 , which are similar to those in Seoul of Korea (Lee
270 et al., 2009), Toulouse of France (Pigeon et al., 2007), and some US cities (Sailor and Lu, 2004;
271 Fan and Sailor, 2005). The regional highest value occurs in Hong Kong, with the value exceeding
272 100 W/m^2 . This value is comparable to those in the most crowded megacities, such as Shanghai
273 (Xie et al., 2016), Tokyo (Ichinose et al., 1999), London (Hamilton et al. 2009; Iamarino et al.
274 2012), and Singapore (Quah and Roth, 2012). In Nanning and Haikou, the annual mean AH fluxes
275 over the whole administrative district are close to 10 W/m^2 . Our spatial distribution of AH based
276 on the population reflects the economic activities in South China, suggesting that our method is
277 effective and the results are reasonable. These results can be supported by other previous
278 investigations (Flanner, 2009; Chen et al., 2012a; 2014; Xie et al., 2015; Lu et al., 2016). So, our
279 AH data can be used in models to investigate their impacts on urban climate and air quality.



280

281

282

283 **Fig. 2. Annual-mean anthropogenic heat fluxes between (101°E, 16°N) and (119°E, 26°N) with the resolution**
 284 **of 2.5 arcmin in 1990 (a), 1995 (b), 2000 (c), 2005 (d), 2010 (e) and 2014 (f), respectively.**

285

286 **Table 3 Annual average anthropogenic heat flux in different administrative district over South China**
 287 **(W/m²)**

Province		This study					
		1990	1995	2000	2005	2010	2014
Guangdong	Regional ^a	0.30	0.48	0.61	1.05	1.53	1.68
	Urban area in PRD	5.11	11.13	14.51	30.82	49.41	58.03
Guangxi	Regional ^a	0.11	0.16	0.17	0.26	0.38	0.44
Hainan	Regional ^a	0.04	0.09	0.14	0.23	0.37	0.49

288 ^a Regional represents the average value over the whole area of a province

289

290 **3.2 Simulation performance**



291 To evaluate the model performance and clarify the better AH parameterization, the modeling
292 results from Fix_AH and Grd_AH are compared with the observation data in two typical months
293 (January and July). Table 4 presents the performance statistics, including the values of monthly
294 mean (Mean), mean bias (MB), root mean squared error (RMSE) and correlative coefficient
295 (COR), which are all quantified for 2-m temperature (T_2), 2-m relative humidity (RH_2), 10-m wind
296 speed (WS_{10}), ozone (O_3), and particles (PM_{10}) in Guangzhou (GZ), Shenzhen (SZ), Nanning
297 (NN), and Haikou (HK).

298 As shown in Table 4, the correlation coefficients (COR) between observations and
299 simulations at four sites are generally about 0.80 for T_2 , over 0.75 for RH_2 , and close to 0.70 for
300 WS_{10} in both January and July (statistically significant at the 95 % confident level). So adding AH
301 in WRF/Chem (Fix_AH and Grd_AH) can well describe the urban meteorological conditions in
302 the typical cities over South China. Compared with the observation records of T_2 , except for
303 Shenzhen in January, both Fix_AH and Grd_AH tend to slightly simulate higher 2-m air
304 temperature at four sites in both months, which can be attributed to the uncertainty of urban
305 canopy and surface parameters (Liao et al., 2015; Xie et al., 2016). These overestimates are
306 acceptable because the MB values are smaller than 1.8 °C in January and smaller than 0.8 °C in
307 July. Moreover, when the gridded AH fluxes are taken into account (Grd_AH), the modeling
308 results of air temperature can be improved, with the mean bias (MB) decreasing by 0.1 - 0.3 °C
309 and the correlation coefficient (COR) increasing by 0.02 - 0.05 (from Fix_AH to Grd_AH). With
310 regards to RH_2 , the modeling values from two simulations (Fix_AH and Grd_AH) are close to the
311 observations. The best simulation occurs in Haikou, and the results at the other three sites are
312 reasonable as well, only with the bias within $\pm 10\%$. These 2-m relative humidity predictions can
313 be improved from Fix_AH to Grd_AH. When we consider the heterogeneity of AH fluxes in
314 Grd_AH, the values of MB and RMSE are closer to 0 and those of COR are closer to 1. For WS_{10} ,
315 because the modeling near-surface wind speed is generally influenced by local underlying surface
316 characteristics more than other meteorological parameters (Liao et al., 2015; Xie et al., 2016), both
317 Fix_AH and Grd_AH slightly overvalue the 10-m wind speed at four sites. In case Fix_AH, the
318 MB for WS_{10} is generally around 1m/s in both months, and the RMSE is less than 2.6 m/s in
319 January and around 2m/s in July. However, the predictions are obviously improved in case
320 Grd_AH. The MB decreases to 0.4-0.9 m/s in January and 0.4-0.7 m/s in July, and the values of
321 COR also increase from 0.68 (Fix_AH) to 0.74 (Grd_AH) in July. These improvements from
322 Fix_AH to Grd_AH for T_2 , RH_2 and WS_{10} predictions suggest that the default value of
323 WRF/Chem for all urban grids overestimates the AH fluxes in these cities, and our gridded AH
324 data as well as the new parameterization scheme can exactly catch the heterogeneity of the heat
325 released from the metropolitans of South China.

326



327

Table 4 Summary of statistics for comparison between simulated and observed hourly averaged meteorological and chemical data in four cities of South China

Case	Vars ^a	Site ^b	Fix_AH						Grid_AH												
			January			July			January			July									
			Mean ^c SIM ^d OBS ^e	MB	RMS E	COR ^f	Mean ^c SIM ^d OBS ^e	MB	RMS E	COR ^f	Mean ^c SIM ^d OBS ^e	MB	RMS E	COR ^f							
T ₂ (°C)	GZ	140	122	1.8	3.1	0.75	29.0	28.4	0.6	4.0	0.72	13.8	12.2	1.6	2.9	0.78	28.8	28.4	0.4	2.1	0.76
	HK	18.9	17.3	1.6	2.0	0.79	29.0	28.4	0.6	1.7	0.79	18.5	17.3	1.3	1.8	0.81	28.9	28.4	0.5	1.6	0.83
RH ₂ (%)	NN	13.9	12.2	1.7	2.9	0.84	28.0	27.7	0.3	2.5	0.77	13.7	12.2	1.4	2.7	0.86	27.9	27.7	0.2	2.0	0.81
	SZ	14.6	14.7	-0.1	1.8	0.84	29.9	29.1	0.8	2.0	0.76	14.4	14.7	-0.3	1.9	0.86	29.6	29.1	0.5	1.9	0.81
WS ₁₀ (m/s)	GZ	64.2	73.5	-9.3	18.5	0.74	68.4	78.8	-10.4	17.9	0.73	66.8	73.5	-6.7	16.8	0.75	71.3	78.8	-7.5	16.8	0.76
	HK	75.6	78.2	-2.5	8.5	0.77	80.6	81.0	-0.3	7.8	0.80	77.0	78.2	-1.1	8.2	0.84	81.4	81.0	0.4	7.7	0.86
O ₃ (ppb)	NN	69.3	77.9	-8.6	18.2	0.74	87.7	83.5	4.2	8.8	0.79	72.3	77.9	-5.6	17.7	0.75	86.5	83.5	3.0	8.9	0.81
	SZ	65.9	63.3	2.6	11.7	0.75	74.2	78.0	-3.8	11.1	0.75	66.5	63.3	3.2	12.3	0.76	75.6	78.0	-2.4	10.5	0.83
PM ₁₀ (µg/m ³)	GZ	3.1	2.4	0.7	1.9	0.75	2.6	1.8	0.8	1.8	0.68	2.8	2.4	0.4	1.3	0.76	2.4	1.8	0.6	1.4	0.74
	HK	4.3	3.3	1.0	2.3	0.74	3.6	2.7	0.9	1.7	0.68	4.2	3.3	0.9	1.8	0.76	3.2	2.7	0.5	1.4	0.74
O ₃ (ppb)	NN	2.5	1.3	1.2	2.3	0.73	2.3	1.5	0.8	2.1	0.68	2.0	1.3	0.7	1.5	0.75	1.9	1.5	0.4	1.2	0.74
	SZ	3.3	2.2	1.1	2.6	0.73	2.8	1.8	1.0	1.8	0.68	2.9	2.2	0.7	1.2	0.75	2.5	1.8	0.7	1.7	0.73
O ₃ (ppb)	GZ	93.7	110.5	-16.8	66.6	0.55	42.2	57.0	-14.8	62.5	0.51	101.3	110.5	-9.2	68.3	0.68	45.3	57.0	-11.7	52.5	0.64
	HK	63.7	75.5	-11.8	48.7	0.58	15.4	25.3	-9.9	25.8	0.51	65.4	75.5	-10.1	48.2	0.71	15.3	25.3	-10.0	21.7	0.63
PM ₁₀ (µg/m ³)	NN	138.4	157.8	-19.4	85.4	0.54	33.8	48.9	-15.1	55.4	0.51	141.7	157.8	-16.1	79.5	0.62	35.4	48.9	-13.5	48.6	0.60
	SZ	64.7	80.0	-15.3	54.2	0.52	28.7	43.9	-15.5	50.1	0.52	67.3	80.0	-12.7	56.5	0.60	31.6	43.9	-12.3	41.0	0.61
O ₃ (ppb)	GZ	21.1	19.6	1.5	13.0	0.53	31.4	28.9	2.5	29.0	0.53	20.3	19.6	0.7	12.2	0.61	31.0	28.9	2.1	25.3	0.63
	HK	32.2	30.9	1.3	14.5	0.53	14.7	11.9	2.8	15.3	0.53	31.9	30.9	1.0	14.1	0.61	14.2	11.9	2.3	13.9	0.63
PM ₁₀ (µg/m ³)	NN	25.6	24.7	0.9	16.7	0.54	19.8	17.3	2.5	12.7	0.54	25.3	24.7	0.6	15.7	0.62	19.1	17.3	1.8	9.0	0.65
	SZ	27.7	28.4	-0.7	14.3	0.54	24.5	20.6	3.9	17.8	0.55	28.0	28.4	-0.4	13.4	0.62	23.7	20.6	3.1	14.3	0.66

^a Vars indicates the variables, including temperature at 2m (T₂), relative humidity at 2m (RH₂), wind speed at 10m (WS₁₀), ozone (O₃) and PM₁₀. ^b Site indicates the city where the observation sites locate, including Guangzhou (GZ), Haikou (HK), Nanning (NN) and Shenzhen (SZ). ^c Mean indicates the monthly average value. ^d SIM indicates the simulation results from WRF/Chem. ^e OBS indicates the observation data. ^f COR indicates the correlation coefficients, with statistically significant at 95% confident level.



332 Table 4 also illustrates the performance of WRF/Chem simulations for the main air pollutants
333 (O_3 and PM_{10}). Obviously, both Fix_AH and Grd_AH can capture the magnitude and temporal
334 variation of main air pollutants in these typical cities over South China, and the simulation with
335 gridded AH fluxes (Grd_AH) can provide better predictions. For Grd_AH, the correlation
336 coefficients (COR) for PM_{10} in all cities are around 0.62 in January and around 0.65 in July
337 (statistically significant at the 95 % confident level). The MB values for PM_{10} are only -0.4 - 1.0
338 $\mu\text{g}/\text{m}^3$ in January and 1.8 -3.1 $\mu\text{g}/\text{m}^3$ in July. With respect to O_3 , the values of MB are -9.2 - -16.1
339 ppb in January and -10.0 - -13.5 ppb in July. These underestimates should be related with the
340 increasing of WS_{10} and the rising of PBL caused by positive biases in T_2 . The uncertainties in
341 emissions of ozone precursors (NO_x and VOCs) may cause these biases as well (Liao et al., 2015;
342 Xie et al., 2016). However, the values of COR for O_3 are 0.60 - 0.71 in January and 0.60 - 0.64 in
343 July (statistically significant at the 95 % confident level), proving that these modeling results are
344 reasonable and acceptable.

345 Fig. 3 presents the monthly-averaged differences of O_3 and PM_{10} between Fix_AH and
346 Grd_AH (Fix_AH minus Grd_AH) at the surface layer over the modeling domain 2 (D02).
347 Obviously, there are some differences between the two simulations that use different AH
348 parameterizations. These differences are more obvious in and around big cities because the AH are
349 related with the human activities. Moreover, the differences in January are higher than those in
350 July, implying that the adding of AH can arouse more atmospheric disturbances in winter. From
351 this point of view, Grd_AH can better describe the spatial and temporal heterogeneity of the
352 impacts of AH on regional air quality.

353 Above all, the WRF/Chem simulation accounting for the temporal and spatial distribution of
354 AH (Grd_AH) has a relatively good capability in simulating urban climate and air quality over
355 South China. So, the differences between the modeling results from Non_AH and Grd_AH can be
356 used to quantify the impacts of anthropogenic heat on meteorology and air pollution.

357 3.3 Impacts of AH on meteorological conditions

358 Fig. 4a-d, Fig. 5a-d, Fig. 6a-b and Fig. 6g-h show the impacts of AH on surface meteorology,
359 which are defined as the monthly-averaged differences of these meteorological factors between
360 Grd_AH and Non_AH (Grd_AH minus Non_AH) at the surface layer over the modeling domain 2.
361 Fig. 4e-f and Fig. 6c-f show the relevant vertical changes of the meteorological factors along the
362 cross-section from (19.1°N, 108.9°E) to (24.8°N, 114.7°E) which is shown as the solid line AB in
363 Fig. 1b.

364

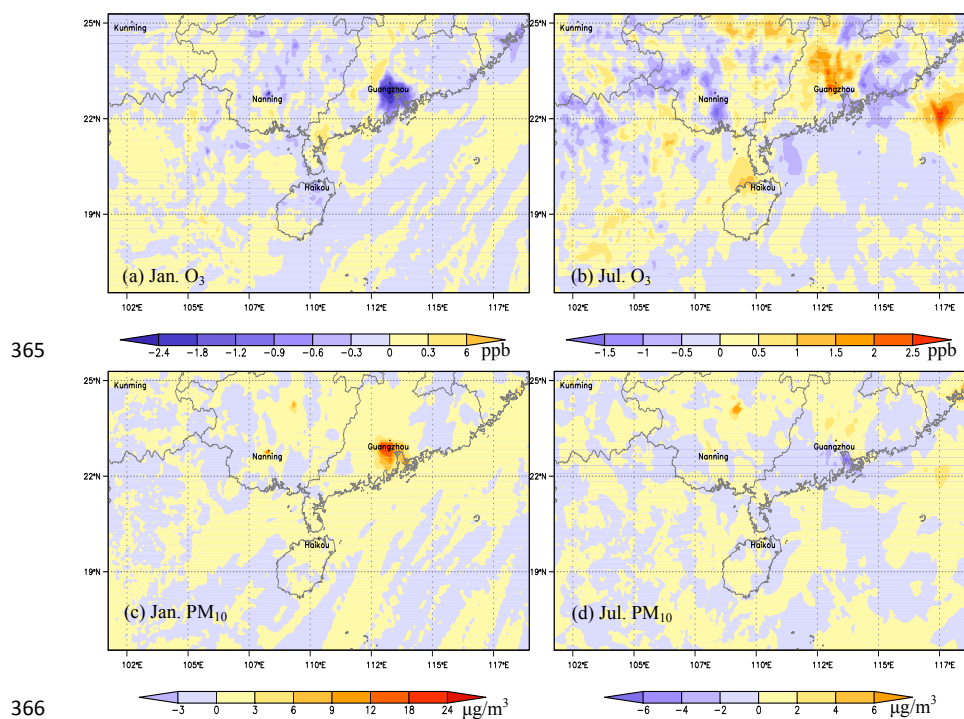


Fig. 3. The spatial distributions of monthly-averaged differences for surface O_3 and PM_{10} between Fix_AH and Grd_AH (Fix_AH minus Grd_AH). (a) and (c) show changes in January. (b) and (d) illustrate variations in July.

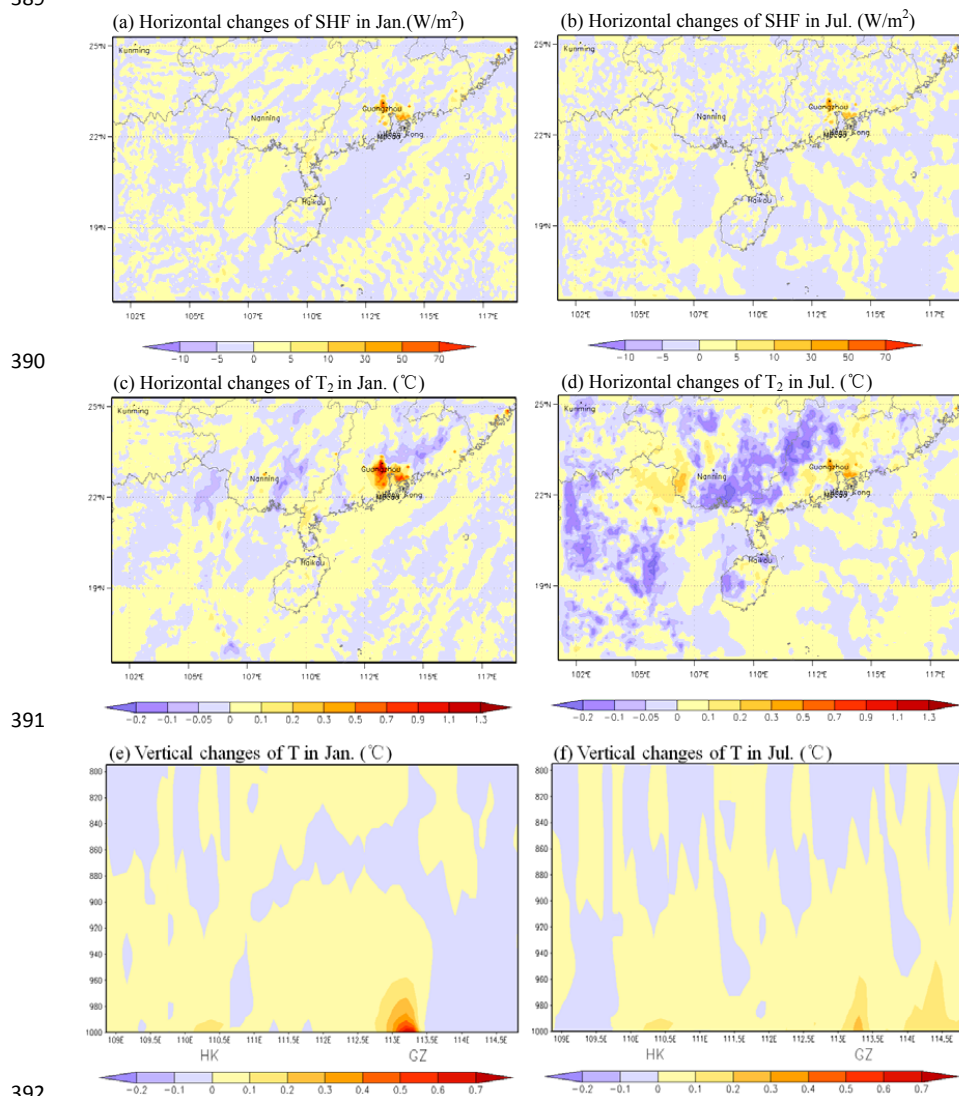
3.3.1 Changes of surface energy and air temperature

372 On account that AH and its diurnal variation are added to the sensible heat item in
373 WRF/Chem, the adding of gridded AH fluxes should increase the modeling results of sensible heat
374 fluxes (SHF) over South China. As shown in Fig. 4a and b, the spatial patterns of SHF changes in
375 both January and July are similar to the spatial distribution of AH fluxes presented in Fig. 2f. The
376 significant increments ($> 10 \text{ W/m}^2$) of SHF over South China usually occur in and around
377 mega-cities. Especially in the PRD city cluster, adding AH can cause SHF to increase by over 50
378 W/m^2 in both January and July.

379 For the 2-m air temperature (T_2) over South China, the AH fluxes can increase their values
380 by adding more surface heat into the atmosphere. As presented in Fig. 4c and d, the patterns of the
381 monthly-averaged T_2 changes are similar to those of SHF (Fig. 4a and b). In the urban areas, the
382 adding of AH can lead to the significant increase of T_2 , which may enhance the Urban Heat Islands.
383 The maximum T_2 changes are usually found in the city centers of the PRD region, with the typical
384 increments over $1.1 \text{ }^\circ\text{C}$ in January and over $0.5 \text{ }^\circ\text{C}$ in July. These findings are comparable to the
385 values estimated for other cities (Fan and Sailor, 2005; Ferguson and Woodbury, 2007; Chen et al.,
386 2009; Zhu et al., 2010; Menberg et al., 2013; Wu and Yang, 2013; Bohnenstengel et al., 2014; Yu



387 et al., 2014; Xie et al., 2016), and can be confirmed by the similar researches in South China
 388 (Meng et al., 2011; Feng et al., 2012; 2014).
 389



392
 393 **Fig. 4.** The monthly-averaged differences between Grd_AH and Non_AH (Grd_AH minus Non_AH) for (a),
 394 (b) the spatial distribution of sensible heat flux (SHF); (c), (d) the spatial distribution of 2-m air temperature
 395 (T_2); (e), (f) the vertical distribution of air temperature (T) from the surface to the 800hPa layer along the
 396 line AB shown in Fig. 1b. Grd_AH and Non_AH represent the simulations with and without AH fluxes. (a),
 397 (c), and (e) show changes in January, while (b), (d), and (f) illustrate variations in July. In (e) and (f), HK
 398 and GZ are the abbreviations for Haikou and Guangzhou, respectively.

399
 400 Fig. 4e and f present the vertical changes of air temperature from the surface to the 800hPa

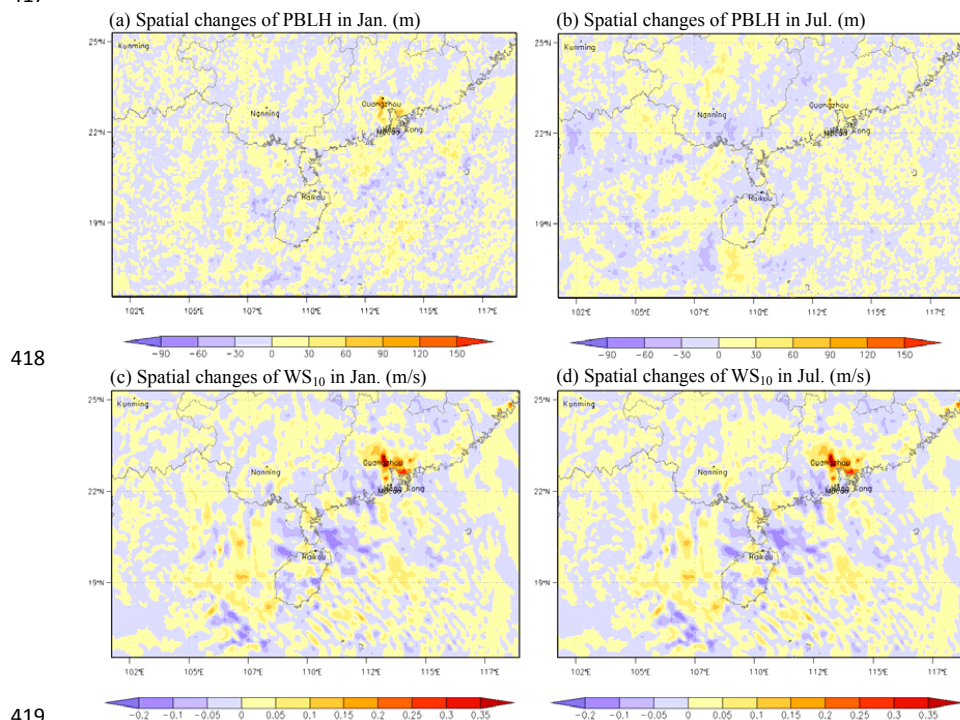


401 layer along the line AB (shown in Fig. 1b), and illustrate that the increases of air temperature
402 causing by adding AH are mainly confined near the surface around the cities (Guangzhou and
403 Haikou). These changes of air temperature in Guangzhou are more obvious than those in Haikou,
404 because the AH emissions are much higher in Guangzhou. Furthermore, T_2 changes in winter (Fig.
405 4e) are more obvious than those in summer (Fig. 4f), with the monthly mean increment of T over
406 0.7°C for January while only around 0.4°C for July in Guangzhou. This phenomenon should be
407 related with the fact that the background heat fluxes are much lower in winter so that the relative
408 increase of T is more obvious.

409 3.3.2 Changes of boundary layer and wind field

410 The warming up of surface air temperature can enhance the vertical air movement in
411 boundary layer (PBL), and thereby can increase the height of boundary layer (PBLH) as well. As
412 shown in Fig. 5a and b, the boundary layer height becomes higher when the AH fluxes are taken
413 into account. The big increments (more than 50m) usually occur in the urban areas of the PRD
414 region. Because relative higher temperature increment in January can induce higher PBL in this
415 cold season, the maximum changing values of PBLH can be 120m for January but only 90m for
416 July.

417



418

419

420 **Fig. 5. The monthly-averaged differences of the height of planetary boundary layer (PBLH) and 10-m wind**
421 **speed (WS_{10}) between Grd_AH and Non_AH (Grd_AH minus Non_AH). Grd_AH and Non_AH represent**
422 **the simulations with and without AH fluxes. (a) and (c) show changes in January, while (b) and (d) illustrate**



423 **variations in July.**

424

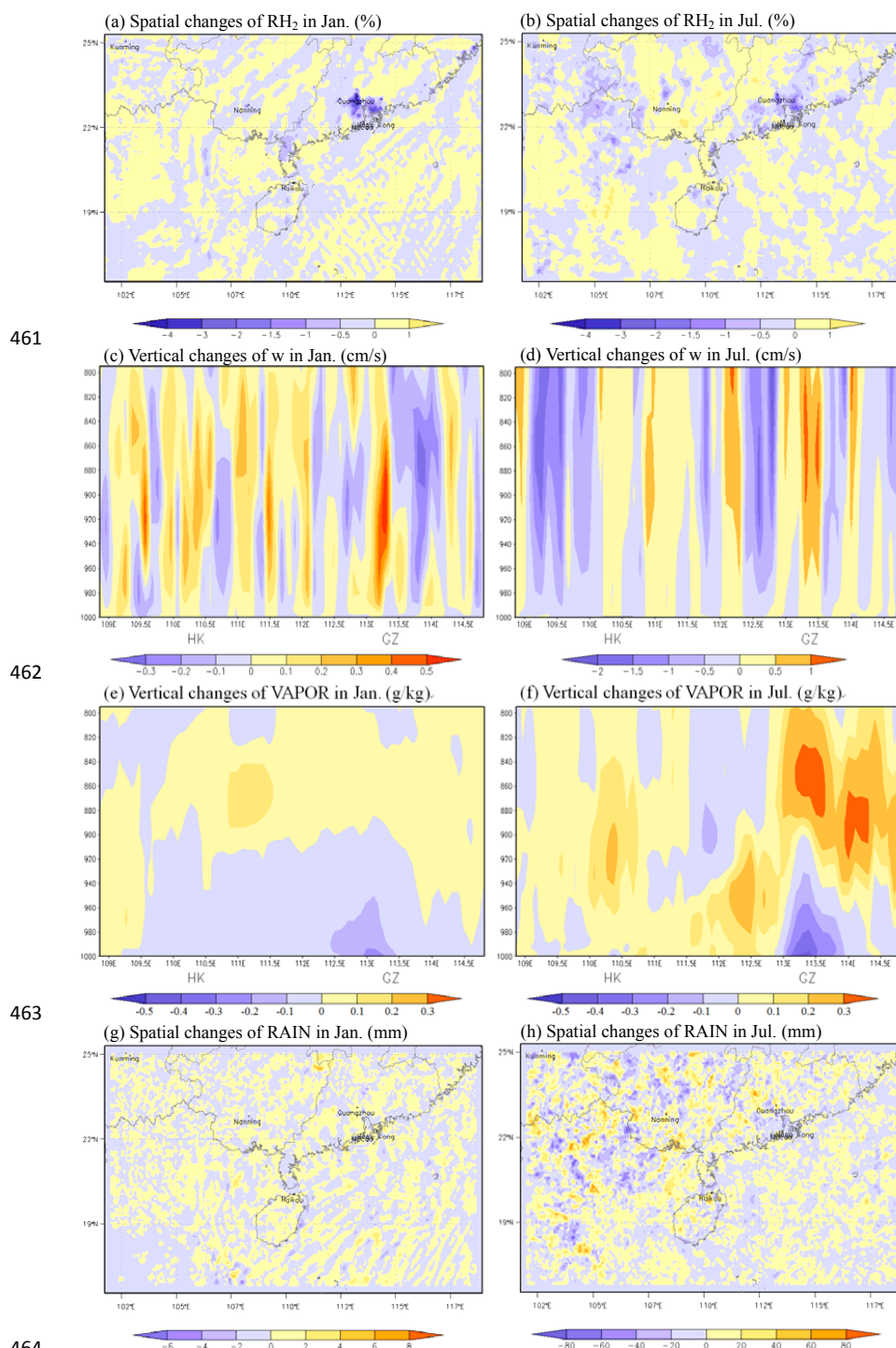
425 Fig. 5c and d show the changes in the 10-m wind speed over South China. Obviously, adding
426 AH can enhance the surface wind in the urban areas. The maximum increase is located in the PRD
427 region, with the values over 0.35 m/s in January and 0.3 m/s in July. In other cities like Chaozhou,
428 Nanning and Haikou, the increments are merely about 0.1 m/s. The warming of air temperature
429 near surface as well as the rising of PBLH induced by adding AH in cities can generate an
430 enhanced urban-breeze circulation. In previous studies, the increases in surface wind speed were
431 considered to be related with this strengthened urban-breeze circulation (Chen et al., 2009; Ryu et
432 al., 2013; Yu et al., 2014; Xie et al., 2016). Our results show that the vertical wind velocities
433 above the Guangzhou and Haikou is enhanced in both January and July (Fig. 6c and d), and the
434 simulated convergence at the surface near these cities increases by 0.04-0.13 /s in January and
435 0.05-0.18 /s in July (not shown). Consequently, we deduce that the enhanced vertical air
436 movement causes the surface stronger convergence and thereby induces higher surface wind
437 speed.

438 **3.3.3 Changes of moisture and rainfall**

439 Fig. 6a and b presents the monthly-averaged differences of 2-m relative humidity (RH_2)
440 between Grd_AH and Non_AH. Obviously, the air near the surface of cities becomes dryer. The
441 negative centers occur in the PRD region, the Chao-Shan area, Haikou and Nanning, which are
442 also the AH emission centers occurring in Fig. 2f. In and around these cities, the reductions of
443 surface RH_2 are -3 to -4% in January and -1% to -2% in July.

444 It was reported that the enhanced vertical air movement can transport more moisture from the
445 surface to the upper layer, and thereby can modify the spatial and vertical distributions of moisture
446 (Xie et al., 2016). This effect mechanism can be clearly illustrated by Fig. 6c-f in this study. As
447 shown in Fig. 6c and d, the vertical wind velocities above Guangzhou and Haikou increase by the
448 values of 0.2 – 0.5 cm/s in January and 0.5 - 1.0 cm/s in July, whereas w decreases in the rural
449 areas with the reductions about -0.3m/s in January and over -0.5 cm/s in July. This pattern means
450 that there are a strengthened upward air flow in cities and a strengthened downward air flow in the
451 surrounding areas, implying that the adding of AH fluxes makes the atmosphere more unstable and
452 tends to form deep convections in troposphere. So, as shown in Fig. 6e and f, more moisture can
453 be transported from the surface to the upper layers. In Guangzhou, for example, the water vapor
454 mixing ratios at the ground level decrease by -0.3g/kg in January and -0.5 g/kg in July, while those
455 at the upper PBL increase by 0.1 g/kg in January and 0.3 g/kg in July. The impact of AH on water
456 vapor is stronger in July. This seasonal difference can be ascribed to the facts that the atmosphere
457 is more stagnant and dryer in winter and more convective and wetter in summer. Furthermore, the
458 changes in Haikou are generally smaller than those in Guangzhou, which can be explained by the
459 fact that the AH emissions are much lower in Haikou.

460



464
 465 **Fig. 6.** The monthly-averaged differences between Grd_AH and Non_AH (Grd_AH minus Non_AH) for (a),
 466 (b) the spatial distribution of 2-m relative humidity (RH₂); (c), (d) the vertical distribution of vertical wind



467 velocity (w); (e), (f) the vertical distribution of water vapor mixing ratio (VAPOR); (g), (h) the spatial
468 distribution of precipitation (RAIN). The vertical cross section is from the surface to the 800hPa layer along
469 the line AB shown in Fig. 1b. Grd_AH and Non_AH represent the simulations with and without AH fluxes.
470 (a), (c), (e), and (g) show changes in January, while (b), (d), (f), and (g) illustrate variations in July. In (c), (d),
471 (e), and (f), HK and GZ are the abbreviations for Haikou and Guangzhou, respectively.

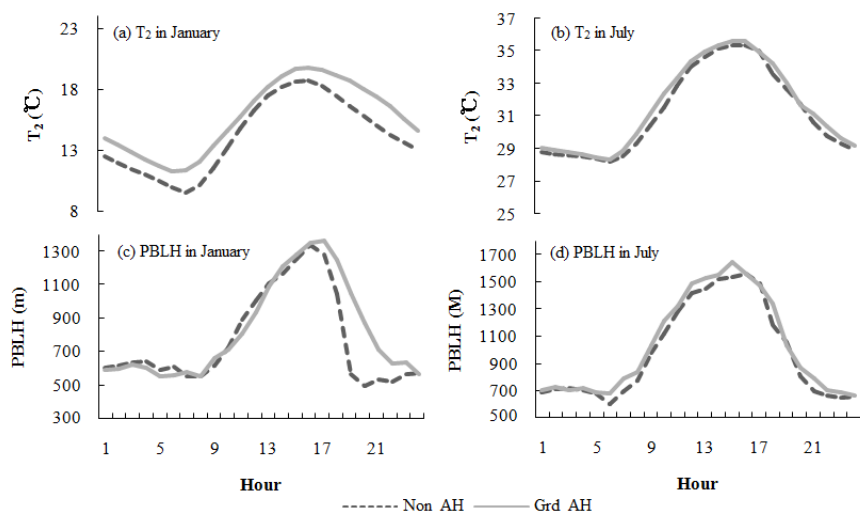
472

473 More moisture transported from surface into the mid-troposphere can increase the
474 precipitation in these urban areas as well. Fig. 6g and h illustrate the enhanced rainfall over South
475 China both in January and July. Because of the negligible accumulative precipitation in winter,
476 there are no significant differences between the Grd_AH and Non_AH simulations for rainfall in
477 January. But in July, the increment of rainfall can be more than 50mm in and around big cities.
478 Moreover, according to the dominant southeast wind in summer, the moisture can be transported
479 to the downwind areas of the PRD city cluster, which causes the increases of rainfall in the
480 northwest part of Guangdong province with the maximum value over 80 mm.

481 3.3.4 Diurnal pattern of the changes

482 In order to better understand the different impacts of AH in the daytime and at night, the
483 monthly-averaged diurnal variations of T_2 and PBLH in January and July over the urban areas in
484 Guangzhou are calculated based on the results from Grd_AH and Non_AH. As shown in Fig. 7a
485 and b, adding AH fluxes can lead to an obvious increase of 2-m air temperature in both months,
486 with the daily mean increase of 1.5°C for January and 0.6 °C for July. The increment of T_2 at night
487 in January (1.69°C) is larger than that in the daytime (1.31°C), whereas the changes during the
488 whole day in July are all around 0.6°C, which suggests that AH can weaken the diurnal T_2
489 variation in winter. With respect to PBLH, the AH fluxes can also result in a higher boundary layer.
490 In July (Fig. 7d), the increment of PBLH nearly keeps a constant value of 54m (4.7%) from
491 morning till night. However, in January (Fig. 7c), the nighttime increase of PBLH is much higher
492 than that in the daytime. This phenomenon may be related with the facts that the absolute PBLH
493 values are lower and the air temperatures increase more in the winter nights.

494



495

496 **Fig. 7.** The monthly-averaged diurnal variations for 2-m air temperature (T_2) and the height of planetary
497 boundary layer (PBLH) over the urban areas in Guangzhou. Grd_AH and Non_AH represent the
498 simulations with and without AH fluxes, respectively. (a) and (c) show diurnal curves in January, while (b)
499 and (d) illustrate those in July.

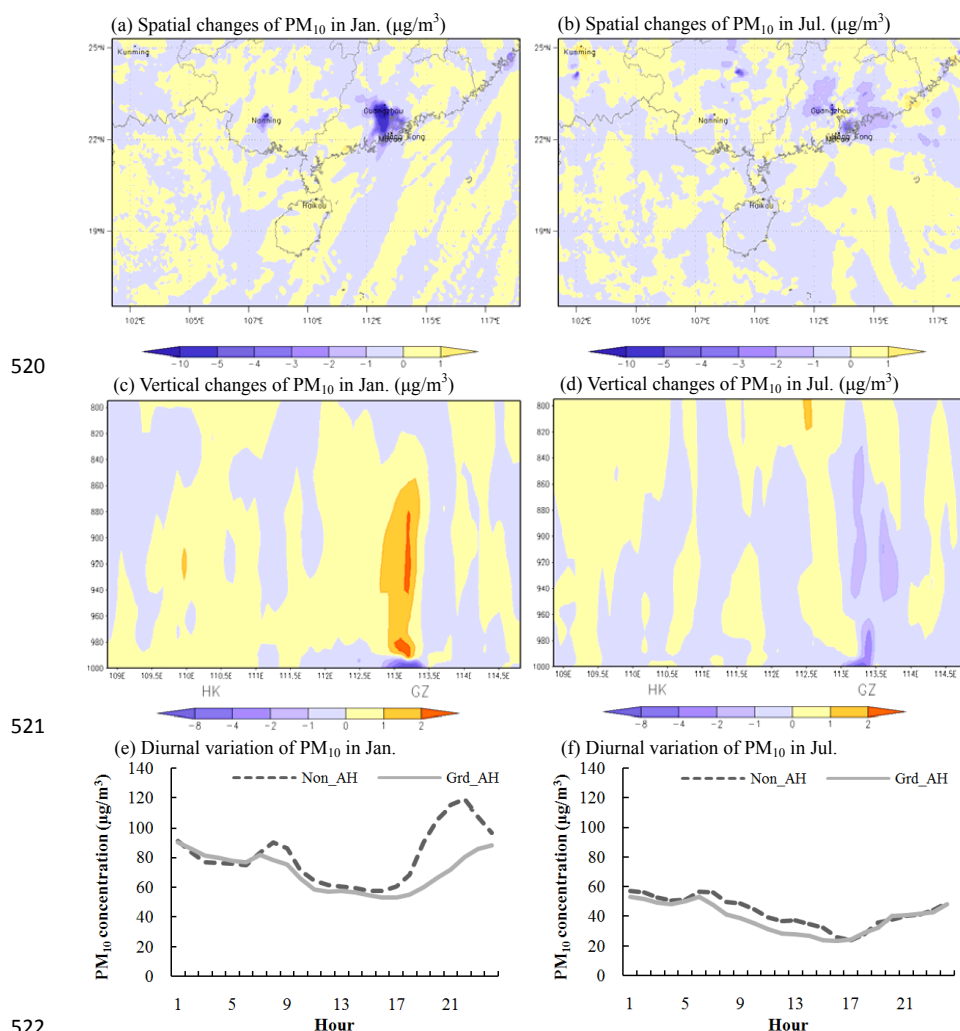
500

501 3.4 Impacts of AH on main air pollutants

502 3.4.1 Changes of the spatial and vertical distribution of PM_{10}

503 Since adding AH changes the meteorology conditions, it can affect the transportation and
504 dispersion of air pollutants as well. Fig. 8a and b show the effects of AH on the spatial distribution
505 of PM_{10} at the surface layer over South China in January and July. They illustrate that the
506 concentrations of PM_{10} decrease in both season near the big cities, including the PRD city cluster,
507 the Chao-shan area, and Nanning etc. The maximum reductions occur in the PRD region, with the
508 monthly mean value over $-10\mu\text{g}/\text{m}^3$ for January and about $-5\mu\text{g}/\text{m}^3$ for July. Compared with the
509 distribution of AH emissions as well as their effects on meteorological conditions, the main causes
510 resulting in the reduction of surface PM_{10} should be attributed to the increase of PBLH, vertical
511 upward air flow and surface wind speed, which can all facilitate PM_{10} transport and dispersion
512 within the urban boundary layer. For another, as shown in Fig. 6h, the rainfall around the PRD
513 cities can increase by 20-40% in July when the AH fluxes are taken into account, so the
514 strengthened wet scavenging in summer may contribute to the decreases of the surface
515 concentrations of PM_{10} as well. The surface reductions of PM_{10} induced by adding AH in the PRD
516 region are smaller than those reported by Xie et al. (2016) in the Yangtze River Delta (YRD)
517 region, which may attributed to the facts that the particle pollution is more severe and the AH
518 emissions as well as their effects on meteorology are more obvious in the YRD region.

519



522 Fig. 8 Impacts of AH fluxes on the concentrations of PM₁₀: (a), (b) the spatial distribution of
 523 monthly-averaged differences for PM₁₀ between Grd_AH and Non_AH (Grd_AH minus Non_AH) at the
 524 surface layer; (c), (d) the vertical distribution of monthly-averaged differences for PM₁₀ between Grd_AH
 525 and Non_AH (Grd_AH minus Non_AH) from the surface to the 800hPa layer along the line AB shown in
 526 Fig. 1b; (e), (f) the monthly-averaged diurnal variations for PM₁₀ concentrations over the urban areas in
 527 Guangzhou. Grd_AH and Non_AH represent the simulations with and without AH fluxes. (a), (c), and (e)
 528 show changes in January, while (b), (d), and (f) illustrate variations in July. In (c) and (d), HK and GZ are
 529 the abbreviations for Haikou and Guangzhou, respectively.
 530
 531

532 Fig. 8c and d present the vertical plots for the changes of PM₁₀ impacted by adding AH
 533 (Grd_AH minus Non_AH) on the cross-sectional line AB shown in Fig. 1b. With respect to the
 534 megacity Guangzhou, the AH fluxes can decrease the concentrations of PM₁₀ near surface and
 535 increase those at the upper layers. This vertical change pattern of PM₁₀ is quite similar to that of
 536 water vapor (Fig. 6e and f), indicating that it is a reflection of the changes in vertical transport



537 pattern due to AH (Yu et al., 2014; Xie et al., 2016). As shown in Fig. 8c for January, the decreases
538 of PM_{10} mainly confined at the surface, with the typical reductions over $-8\mu\text{g}/\text{m}^3$. Meanwhile, there
539 are obvious increases of PM_{10} concentrations at the upper levels, with the increments over $2\mu\text{g}/\text{m}^3$
540 from the 980hPa layer to the 850hPa layer (approximately from 500m to 1500m). But for July (Fig.
541 8d), from the surface to the 850hPa layer over Guangzhou, the PM_{10} concentrations are all reduced
542 over $-1\mu\text{g}/\text{m}^3$, with the maximum values over $-4\mu\text{g}/\text{m}^3$ on the ground. The increasing zones only
543 occur at the upper layers above 1.5km, with the increments over $1\mu\text{g}/\text{m}^3$. This significant seasonal
544 difference for the vertical distribution of PM_{10} changes over Guangzhou should be related with the
545 fact that the atmosphere is more unstable and convective in summer than in winter, which can be
546 further proven by the phenomenon that the enhanced upward air movement in July is stronger than
547 that in January (shown in Fig. 6e and f). It should be noted that the vertical changes of PM_{10} in
548 Haikou are indistinctive, implying that the surface air pollutants cannot be remarkably affected by
549 adding AH if the heat emission fluxes are less than $10\text{ w}/\text{m}^2$. Furthermore, the low particle
550 pollution level may be another cause for the negligible vertical changes of PM_{10} in Haikou.

551 Fig. 8e and f show the monthly-averaged diurnal variations of surface PM_{10} from the
552 Grd_AH and Non_AH simulations over the urban areas in Guangzhou. Obviously, the adding of
553 AH fluxes can lead to the decrease of surface PM_{10} concentrations, with the daily mean value of
554 $-10.4\mu\text{g}/\text{m}^3$ for January and $-4.3\mu\text{g}/\text{m}^3$ for July. There are significant differences between the
555 impacts of AH in the daytime and those at night. In July (Fig. 8f), the decreases mainly occur from
556 6:00 to 17:00. In January (Fig. 8e), the decreases are $-8.8\mu\text{g}/\text{m}^3$ from 8:00 to 18:00 and $-11.9\mu\text{g}/\text{m}^3$
557 from 19:00 to 7:00, with the maximum reduction of $-36.9\mu\text{g}/\text{m}^3$ at 21:00. This pattern has a
558 reverse correlation with the changes of PBLH shown in Fig. 7c and d, which also manifests the
559 important role of vertical air movement in the changes of PM_{10} .

560 3.4.2 Changes of the spatial and vertical distribution of O_3

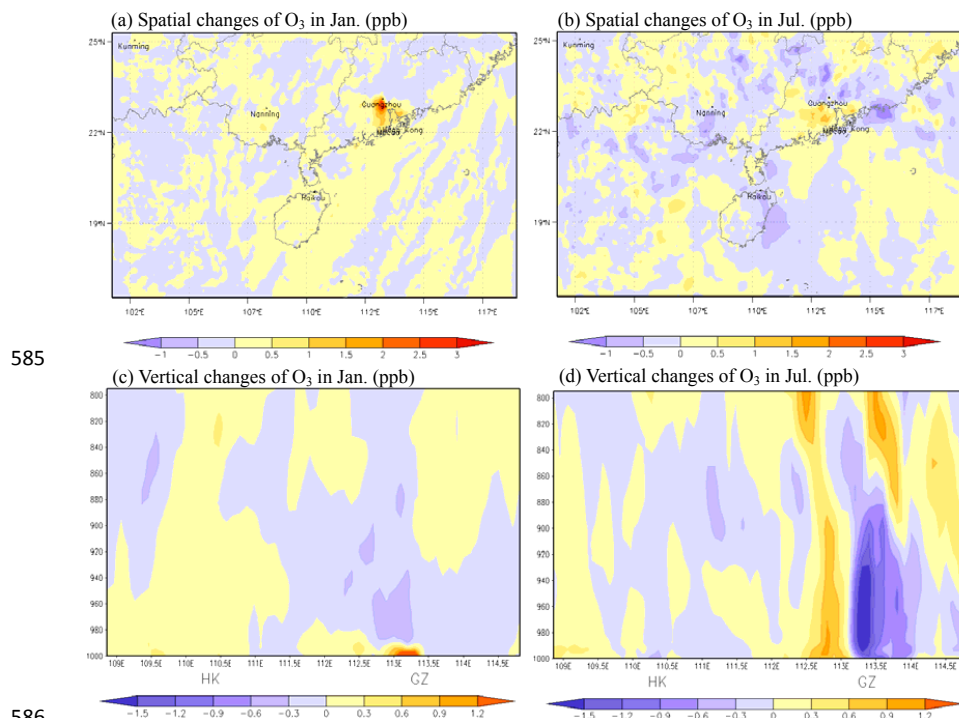
561 Fig. 9a and b present the effects of AH on the spatial distribution of O_3 at the surface layer
562 over South China. The results show that the increases of surface O_3 level can be seen in megacities
563 for both January and July. In January (Fig. 9a), the maximum O_3 differences occur in the big cities
564 of the PRD region, with the monthly mean increment over 2.5ppb. In July (Fig. 9b), the increasing
565 areas become larger, but with the high values close to 1 ppb in and around the cities. This
566 changing pattern is similar to the findings reported in Seoul (Ryu et al., 2013), Beijing (Yu et al.,
567 2014) and the cities in the YRD region (Xie et al., 2016).

568 Fig. 9c and d show the effects of AH on the vertical distribution of O_3 from the surface to the
569 800hPa layer along the line AB (illustrated in Fig. 1b). For the urban areas of Haikou, the vertical
570 changes of O_3 are all within ± 0.2 ppb, which means that low AH emissions in this city ($<10\text{ w}/\text{m}^2$)
571 cannot remarkably affect the physical and chemical formation of O_3 . However, over the urban
572 areas of big city Guangzhou, the vertical distribution of O_3 concentrations can be noticeably
573 changed. In January (Fig. 9c), O_3 increases at the surface while decreases at the upper levels. The
574 increases of O_3 concentrations are limited within 300m above the surface ($<995\text{ hPa}$) over the



575 urban areas, with the high values over 2.5 ppb. The maximum decreases of O₃ concentrations
576 occur from the 990hPa layer to the 860hPa layer (approximately from 400m to 1500m), and the
577 typical reductions are about 0.3 ppb. This change pattern in winter for Guangzhou is similar to the
578 findings reported in Shanghai and Hangzhou (Xie et al., 2016). But for July, the vertical change
579 pattern of O₃ above Guangzhou is totally different. As illustrated in Fig. 9d, O₃ concentrations
580 decrease at the lower layers while increase at the upper levels. The decreases occur from the
581 surface to the 850hPa layer (about 1.5 km) with the reduction values of -1 to -1.5ppb, and the
582 increases appear at the upper layers as well as the surrounding air columns around Guangzhou
583 with the increment about 0.9-1.2 ppb.

584



585

586

587 **Fig. 9. Impacts of AH fluxes on the concentrations of O₃: (a), (b) the spatial distribution of**
588 **monthly-averaged differences for O₃ between Grd_AH and Non_AH (Grd_AH minus Non_AH) at the**
589 **surface layer; (c), (d) the vertical distribution of monthly-averaged differences for O₃ between Grd_AH and**
590 **Non_AH (Grd_AH minus Non_AH) from the surface to the 800hPa layer along the line AB shown in Fig. 1b.**
591 **Grd_AH and Non_AH represent the simulations with and without AH fluxes. (a) and (c) show changes in**
592 **January, while (b) and (d) illustrate variations in July. In (c) and (d), HK and GZ are the abbreviations for**
593 **Haikou and Guangzhou, respectively.**

594

595 The mechanism how the AH fluxes influence the spatial and vertical distribution of O₃ is
596 more complicated than that for PM₁₀. Only taking the physical effects that just impact O₃ transport
597 and dispersion into account, we can merely deduce that O₃ is seemingly reduced at the surface and



598 may increase at the upper layers, because the increase of surface wind speed can facilitate O₃
599 advection transport and the rising up of PBLH can lead to O₃ dilution. However, O₃ is a secondary
600 air pollutant produced by a series of complex chemical reactions that are also deeply affected by
601 the ambient meteorological conditions. So, the chemical effects can play an important role in O₃
602 changes as well. For example, the increases of air temperature induced by adding AH can
603 accelerate O₃ production rate. So it can directly increase the O₃ concentrations near the surface
604 (referred to as the direct chemical effect hereafter). Moreover, because of the O₃ sensitivity in the
605 daytime and the NO_x titration at night, O₃ formation is inextricably linked with NO_x (referred to as
606 indirect chemical effect hereafter). As shown in Fig. 10, due mainly to the increases of PBLH and
607 upward air flow caused by adding AH, NO_x can decrease at ground level and increase at upper
608 layers in both January and July. Then when the process of NO_x titration predominate the O₃
609 chemistry at night, less NO_x consumes less O₃ and leaves more O₃ at the surface while more NO_x
610 consumes more O₃ and reduce O₃ at the upper layers. For the daytime, because O₃ formation is
611 sensitive to VOC over the cities in South China (Xie et al., 2014), the decrease in surface NO_x can
612 lead to a slight increase in O₃ while the increase of NO_x at upper layers can result in the O₃
613 decrease. In January over Guangzhou, these direct and indirect chemical effects should play a
614 more important role in O₃ changes than the physical effects, and thereby O₃ increases at ground
615 level and decreases at upper layers. But in July, the physical effects should be the governing factor
616 and cause the different pattern of O₃ changes in Guangzhou.

617 In the previous study on the O₃ variations induced by adding AH, it was found that the
618 vertical changing patterns of O₃ over the YRD region in both January and July are always the
619 same as the pattern shown in the winter of Guangzhou (Xie et al., 2016). Comparing the vertical
620 changes of w for July in Guangzhou and those in Shanghai or Hangzhou, we can tell that the AH
621 fluxes can induce stronger upward air movement in the cities of South China, which may be
622 related with their special topographic and climatic features, and thereby more O₃ below the
623 850hPa layer is transported to the upper layers or to the surrounding areas of Guangzhou. On the
624 other hand, the rise of air temperature is smaller in Guangzhou than those in the YRD cities, so
625 there is no enough produced O₃ to compensate the loss of O₃ on the ground. Consequently,
626 impacted by adding AH, O₃ decreases at the surface while increases at the upper layers in the
627 summer of Guangzhou.

628

629 4. Conclusions

630 Anthropogenic heat (AH) fluxes related with the human activities can change the urban
631 circulation and thereby affect the air pollution in and around cities. In this paper, we carry out
632 systematic analyses to study the changes of meteorological conditions induced by AH and their
633 effects on the concentrations of PM₁₀, NO_x and O₃ in South China. Firstly, the temporal and spatial
634 distribution of AH emissions is estimated by a top-down energy inventory method. Secondly, the
635 AH parameterization in WRF/Chem is modified to adopt the gridded AH data with the temporal

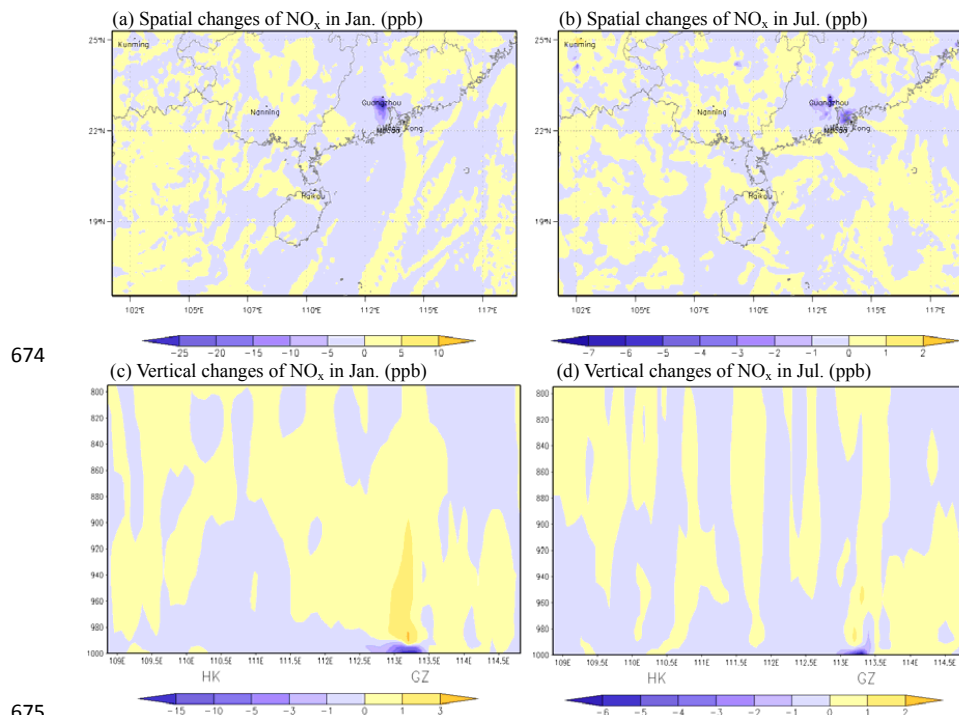


636 variation. Finally, the WRF/Chem simulations are performed, and the differences between the
637 cases with and without adding AH are analyzed to quantify the impacts of AH.

638 The results show that high AH fluxes generally occur in and around the cities. In 2014, the
639 regional mean values of AH over Guangdong, Guangxi and Hainan province are 1.68, 0.44 and
640 0.49 W/m², while the typical values in the urban areas of the PRD region can reach 58.03w/m².
641 The model results of WRF/Chem fit the observations well. Adding the gridded AH emissions can
642 better describe the heterogeneous impacts of AH on regional meteorology and air quality. When
643 AH fluxes are taken into account, the urban heat island and urban-breeze circulations in the big
644 cities are significantly changed. In the PRD city cluster, 2-m air temperature rises up by 1.1°C in
645 January and over 0.5°C in July, the boundary layer height increases by 120m in January and 90m
646 in July, and 10-m wind speed is enhanced over 0.35 m/s in January and 0.3 m/s in July. The
647 enhanced vertical movement can transport more moisture to higher levels, and causes the
648 accumulative precipitation to increase by 20-40% over the megacities in July. Influenced by the
649 modifications of meteorological conditions, the spatial and vertical distribution of air pollutants is
650 modified as well. The concentrations of PM₁₀ and NO_x decrease near surface while increase at the
651 upper levels over the big cities in the PRD region, which are mainly related with the higher PBLH,
652 stronger upward air flower, and higher surface wind speed. Because the direct chemical effect (the
653 rising up of air temperature directly accelerates surface O₃ formation) and the indirect chemical
654 effect (the decrease in NO_x at the ground results in the increase of surface O₃) play a more
655 important role than the physical effects in winter, the surface O₃ concentrations can increase in
656 January with maximum changes over 2.5ppb in the megacities. However, in July, the vertical
657 changes of O₃ concentrations induced by adding AH show a different pattern, with reductions at
658 the lower layers and increments at the upper layers over Guangzhou. This phenomenon should be
659 attributed to the fact that the physical effects (enhanced upward movement caused by AH) become
660 the dominant factor in summer.

661 There is an important question asked many times by scientists about whether anthropogenic
662 heat emissions contribute to global warming. Although the answers are probably negative, the
663 systematic analyses of AH over South China in this paper can enhance the understanding of the
664 magnitude of AH emission from megacities and its impact on regional meteorology and
665 atmospheric chemistry. Compared with the effects from urban land use (Wang et al., 2007; 2009b;
666 Feng et al., 2012; Chen et al., 2014b; Li et al., 2014; 2016; Liao et al., 2015; Zhu et al., 2015), the
667 impacts of AH are relative small. Especially in some cities with less air pollution and AH
668 emissions, such as Haikou, the effects of AH on air quality may be ignored. But our results also
669 clearly show that the meteorology and air pollution predictions in and around big cities are highly
670 sensitive to the anthropogenic heat inputs. Thus, for further understanding of urban atmospheric
671 environment issues, more studies of the anthropogenic heat release in megacities should be better
672 considered.

673



674

675

676 **Fig. 10. Impacts of AH fluxes on the concentrations of NO_x:** (a), (b) the spatial distribution of
677 monthly-averaged differences for NO_x between Grd_AH and Non_AH (Grd_AH minus Non_AH) at the
678 surface layer; (c), (d) the vertical distribution of monthly-averaged differences for NO_x between Grd_AH
679 and Non_AH (Grd_AH minus Non_AH) from surface to 800 hPa layer along the line AB shown in Fig. 1b.
680 Grd_AH and Non_AH represent the simulations with and without AH fluxes. (a) and (c) show changes in
681 January, while (b) and (d) illustrate variations in July. In (c) and (d), HK and GZ are the abbreviations for
682 Haikou and Guangzhou, respectively.

683

684 Acknowledgments

685 This work was supported by the National Natural Science Foundation of China (41475122,
686 91544230), Key Laboratory of South China Sea Meteorological Disaster Prevention and
687 Mitigation of Hainan Province (SCSF201401), the National Special Fund for Environmental
688 Protection Research in the Public Interest (201409008), the National Science Foundation of
689 Jiangsu Province (BE2015151), and EU 7th Framework Marie Curie Actions IRSES project
690 REQUA (PIRSSES-GA-2013-612671). The authors would like to thank the anonymous reviewers
691 for their constructive and precious comments on this manuscript.

692

693 References

694 Ackermann, I. J., Hass, H., Memmesheimer, M., Ebel, A., Binkowski, F. S., and Shankar, U.: Modal aerosol
695 dynamics model for Europe: Development and first applications, *Atmos Environ*, 32, 2981-2999, Doi
696 10.1016/S1352-2310(98)00006-5, 1998.
697 Akbari, H., Pomerantz, M., and Taha, H.: Cool surfaces and shade trees to reduce energy use and improve air



- 698 quality in urban areas, *Sol Energy*, 70, 295-310, Doi 10.1016/S0038-092x(00)00089-X, 2001.
- 699 Allen, L., Lindberg, F., and Grimmond, C. S. B.: Global to city scale urban anthropogenic heat flux: model and
700 variability, *International Journal Of Climatology*, 31, 1990-2005, 10.1002/joc.2210, 2011.
- 701 Balzarini, A., Pirovano, G., Honzak, L., Zabkar, R., Curci, G., Forkel, R., Hirtl, M., San Jose, R., Tuccella, P., and
702 Grell, G. A.: WRF-Chem model sensitivity to chemical mechanisms choice in reconstructing aerosol optical
703 properties, *Atmos Environ*, 115, 604-619, 10.1016/j.atmosenv.2014.12.033, 2015.
- 704 Block, A., Keuler, K., and Schaller, E.: Impacts of anthropogenic heat on regional climate patterns, *Geophys Res*
705 *Lett*, 31, Artn L12211
706 10.1029/2004gl019852, 2004.
- 707 Bohnenstengel, S. I., Hamilton, I., Davies, M., and Belcher, S. E.: Impact of anthropogenic heat emissions on
708 London's temperatures, *Q J Roy Meteor Soc*, 140, 687-698, 10.1002/qj.2144, 2014.
- 709 Chan, C. K., and Yao, X.: Air pollution in mega cities in China, *Atmos Environ*, 42, 1-42,
710 10.1016/j.atmosenv.2007.09.003, 2008.
- 711 Chen, F., and Dudhia, J.: Coupling an advanced land surface-hydrology model with the Penn State-NCAR MM5
712 modeling system. Part I: Model implementation and sensitivity, *Mon Weather Rev*, 129, 569-585, Doi
713 10.1175/1520-0493(2001)129<0569:Caalsh>2.0.Co;2, 2001.
- 714 Chen, Y., Jiang, W. M., Zhang, N., He, X. F., and Zhou, R. W.: Numerical simulation of the anthropogenic heat
715 effect on urban boundary layer structure, *Theor Appl Climatol*, 97, 123-134, 10.1007/s00704-008-0054-0, 2009.
- 716 Chen, F., Kusaka, H., Bornstein, R., Ching, J., Grimmond, C. S. B., Grossman-Clarke, S., Loridan, T., Manning, K.
717 W., Martilli, A., Miao, S. G., Sailor, D., Salamanca, F. P., Taha, H., Tewari, M., Wang, X. M., Wyszogrodzki, A.
718 A., and Zhang, C. L.: The integrated WRF/urban modelling system: development, evaluation, and applications to
719 urban environmental problems, *International Journal Of Climatology*, 31, 273-288, 10.1002/joc.2158, 2011.
- 720 Chen, B., Shi, G. Y., Wang, B., Zhao, J. Q., and Tan, S. C.: Estimation of the anthropogenic heat release
721 distribution in China from 1992 to 2009, *Acta Meteorol Sin*, 26, 507-515, 10.1007/s13351-012-0409-y, 2012.
- 722 Chen, B., Dong, L., Shi, G. Y., Li, L. J., and Chen, L. F.: Anthropogenic Heat Release: Estimation of Global
723 Distribution and Possible Climate Effect, *J Meteorol Soc Jpn*, 92A, 157-165, 10.2151/jmsj.2014-A10, 2014.
- 724 Chen, B., Yang, S., Xu, X. D., and Zhang, W.: The impacts of urbanization on air quality over the Pearl River
725 Delta in winter: roles of urban land use and emission distribution, *Theor Appl Climatol*, 117, 29-39,
726 10.1007/s00704-013-0982-1, 2014.
- 727 Civerolo, K., Hogrefe, C., Lynn, B., Rosenthal, J., Ku, J. Y., Solecki, W., Cox, J., Small, C., Rosenzweig, C.,
728 Goldberg, R., Knowlton, K., and Kinney, P.: Estimating the effects of increased urbanization on surface
729 meteorology and ozone concentrations in the New York City metropolitan region, *Atmos Environ*, 41,
730 1803-1818, 10.1016/j.atmosenv.2006.10.076, 2007.
- 731 Crutzen, P. J.: New Directions: The growing urban heat and pollution "island" effect - impact on chemistry and
732 climate, *Atmos Environ*, 38, 3539-3540, 10.1016/j.atmosenv.2004.03.032, 2004.
- 733 Fan, H. L., and Sailor, D. J.: Modeling the impacts of anthropogenic heating on the urban climate of Philadelphia:
734 a comparison of implementations in two PBL schemes, *Atmos Environ*, 39, 73-84,
735 10.1016/j.atmosenv.2004.09.031, 2005.
- 736 Fang, M., Chan, C. K., and Yao, X. H.: Managing air quality in a rapidly developing nation: China, *Atmos Environ*,
737 43, 79-86, 10.1016/j.atmosenv.2008.09.064, 2009.
- 738 Feng, J. M., Wang, Y. L., Ma, Z. G., and Liu, Y. H.: Simulating the Regional Impacts of Urbanization and
739 Anthropogenic Heat Release on Climate across China, *J Climate*, 25, 7187-7203, 10.1175/Jcli-D-11-00333.1,
740 2012.
- 741 Feng, J. M., Wang, J., and Yan, Z. W.: Impact of Anthropogenic Heat Release on Regional Climate in Three Vast
742 Urban Agglomerations in China, *Adv Atmos Sci*, 31, 363-373, 10.1007/s00376-013-3041-z, 2014.



- 743 Ferguson, G., and Woodbury, A. D.: Urban heat island in the subsurface, *Geophys Res Lett*, 34, Artn L23713
744 10.1029/2007gl032324, 2007.
- 745 Flanner, M. G.: Integrating anthropogenic heat flux with global climate models, *Geophys Res Lett*, 36, Artn
746 L02801
747 10.1029/2008gl036465, 2009.
- 748 Grell, G. A., and Devenyi, D.: A generalized approach to parameterizing convection combining ensemble and data
749 assimilation techniques, *Geophys Res Lett*, 29, Artn 1693
750 10.1029/2002gl015311, 2002.
- 751 Grell, G. A., Peckham, S. E., Schmitz, R., McKeen, S. A., Frost, G., Skamarock, W. C., and Eder, B.: Fully
752 coupled "online" chemistry within the WRF model, *Atmos Environ*, 39, 6957-6975,
753 10.1016/j.atmosenv.2005.04.027, 2005.
- 754 Group, W. B.: East asia's changing urban landscape: measuring a decade of spatial growth, World Bank,
755 Washington Dc, 2015.
- 756 Guenther, A., Karl, T., Harley, P., Wiedinmyer, C., Palmer, P. I., and Geron, C.: Estimates of global terrestrial
757 isoprene emissions using MEGAN (Model of Emissions of Gases and Aerosols from Nature), *Atmos Chem Phys*,
758 6, 3181-3210, 2006.
- 759 Hamilton, I. G., Davies, M., Steadman, P., Stone, A., Ridley, I., and Evans, S.: The significance of the
760 anthropogenic heat emissions of London's buildings: A comparison against captured shortwave solar radiation,
761 *Build Environ*, 44, 807-817, 10.1016/j.buildenv.2008.05.024, 2009.
- 762 Iamarino, M., Beever, S., and Grimmond, C. S. B.: High-resolution (space, time) anthropogenic heat emissions:
763 London 1970-2025, *International Journal Of Climatology*, 32, 1754-1767, 10.1002/joc.2390, 2012.
- 764 Ichinose, T., Shimodozono, K., and Hanaki, K.: Impact of anthropogenic heat on urban climate in Tokyo, *Atmos
765 Environ*, 33, 3897-3909, Doi 10.1016/S1352-2310(99)00132-6, 1999.
- 766 Janjic, Z. I.: The Step-Mountain Eta Coordinate Model - Further Developments Of the Convection, Viscous
767 Sublayer, And Turbulence Closure Schemes, *Mon Weather Rev*, 122, 927-945, Doi
768 10.1175/1520-0493(1994)122<0927:Tsmecm>2.0.Co;2, 1994.
- 769 Jiang, X. Y., Wiedinmyer, C., Chen, F., Yang, Z. L., and Lo, J. C. F.: Predicted impacts of climate and land use
770 change on surface ozone in the Houston, Texas, area, *J Geophys Res-Atmos*, 113, Artn D20312
771 10.1029/2008jd009820, 2008.
- 772 Kim, H. J., and Wang, B.: Sensitivity of the WRF Model Simulation of the East Asian Summer Monsoon in 1993
773 to Shortwave Radiation Schemes and Ozone Absorption, *Asia-Pac J Atmos Sci*, 47, 167-180,
774 10.1007/s13143-011-0006-y, 2011.
- 775 Lee, S. H., Song, C. K., Baik, J. J., and Park, S. U.: Estimation of anthropogenic heat emission in the Gyeong-In
776 region of Korea, *Theor Appl Climatol*, 96, 291-303, 10.1007/s00704-008-0040-6, 2009.
- 777 Li, M. M., Song, Y., Huang, X., Li, J. F., Mao, Y., Zhu, T., Cai, X. H., and Liu, B.: Improving mesoscale modeling
778 using satellite-derived land surface parameters in the Pearl River Delta region, China, *J Geophys Res-Atmos*,
779 119, 6325-6346, 10.1002/2014JD021871, 2014.
- 780 Li, M. M., Song, Y., Mao, Z. C., Liu, M. X., and Huang, X.: Impacts of thermal circulations induced by
781 urbanization on ozone formation in the Pearl River Delta region, China, *Atmos Environ*, 127, 382-392,
782 10.1016/j.atmosenv.2015.10.075, 2016.
- 783 Liao, J. B., Wang, T. J., Jiang, Z. Q., Zhuang, B. L., Xie, M., Yin, C. Q., Wang, X. M., Zhu, J. L., Fu, Y., and
784 Zhang, Y.: WRF/Chem modeling of the impacts of urban expansion on regional climate and air pollutants in
785 Yangtze River Delta, China, *Atmos Environ*, 106, 204-214, 10.1016/j.atmosenv.2015.01.059, 2015.
- 786 Lin, Y. L., Farley, R. D., and Orville, H. D.: Bulk Parameterization Of the Snow Field In a Cloud Model, *J Clim
787 Appl Meteorol*, 22, 1065-1092, Doi 10.1175/1520-0450(1983)022<1065:Bspotsf>2.0.Co;2, 1983.



- 788 Liu, M., Wang, H., Wang, H., Oda, T., Zhao, Y., Yang, X., Zang, R., Zang, B., Bi, J., and Chen, J.: Refined
789 estimate of China's CO₂ emissions in spatiotemporal distributions, *Atmos Chem Phys*, 13, 10873-10882,
790 10.5194/acp-13-10873-2013, 2013.
- 791 Liu, Q., Lam, K. S., Jiang, F., Wang, T. J., Xie, M., Zhuang, B. L., and Jiang, X. Y.: A numerical study of the
792 impact of climate and emission changes on surface ozone over South China in autumn time in 2000-2050, *Atmos*
793 *Environ*, 76, 227-237, 10.1016/j.atmosenv.2013.01.030, 2013.
- 794 Lo, J. C. F., Lau, A. K. H., Chen, F., Fung, J. C. H., and Leung, K. K. M.: Urban modification in a mesoscale
795 model and the effects on the local circulation in the Pearl River Delta region, *J Appl Meteorol Clim*, 46, 457-476,
796 10.1175/Jam2477.1, 2007.
- 797 Lu, X., Chow, K. C., Yao, T., Lau, A. K. H., and Fung, J. C. H.: Effects of urbanization on the land sea breeze
798 circulation over the Pearl River Delta region in winter, *International Journal Of Climatology*, 30, 1089-1104,
799 10.1002/joc.1947, 2010.
- 800 Lu, Y., Wang, Q. G., Zhang, Y. Y., Sun, P., and Qian, Y.: An estimate of anthropogenic heat emissions in China,
801 *International Journal Of Climatology*, 36, 1134-1142, 10.1002/joc.4407, 2016.
- 802 Madronich, S.: Photodissociation In the Atmosphere .1. Actinic Flux And The Effects Of Ground Reflections And
803 Clouds, *J Geophys Res-Atmos*, 92, 9740-9752, Doi 10.1029/Jd092id08p09740, 1987.
- 804 Menberg, K., Bayer, P., Zosseder, K., Rumohr, S., and Blum, P.: Subsurface urban heat islands in German cities,
805 *Sci Total Environ*, 442, 123-133, 10.1016/j.scitotenv.2012.10.043, 2013.
- 806 Meng, W. G., Zhang, Y. X., Li, J. N., Lin, W. S., Dai, G. F., and Li, H. R.: Application Of Wrf/Ucm In the
807 Simulation Of a Heat Wave Event And Urban Heat Island around Guangzhou, *J Trop Meteorol*, 17, 257-267,
808 10.3969/j.issn.1006-8775.2011.03.007, 2011.
- 809 Mirzaei, P. A., and Haghghat, F.: Approaches to study Urban Heat Island - Abilities and limitations, *Build*
810 *Environ*, 45, 2192-2201, 10.1016/j.buildenv.2010.04.001, 2010.
- 811 Mlawer, E. J., Taubman, S. J., Brown, P. D., Iacono, M. J., and Clough, S. A.: Radiative transfer for
812 inhomogeneous atmospheres: RRTM, a validated correlated-k model for the longwave, *J Geophys Res-Atmos*,
813 102, 16663-16682, Doi 10.1029/97jd00237, 1997.
- 814 Oke, T. R.: The Urban Energy-Balance, *Prog Phys Geog*, 12, 471-508, Doi 10.1177/030913338801200401, 1988.
- 815 Pigeon, G., Legain, D., Durand, P., and Masson, V.: Anthropogenic heat release in an old European agglomeration
816 (Toulouse, France), *International Journal Of Climatology*, 27, 1969-1981, 10.1002/joc.1530, 2007.
- 817 Quah, A. K. L., and Roth, M.: Diurnal and weekly variation of anthropogenic heat emissions in a tropical city,
818 Singapore, *Atmos Environ*, 46, 92-103, 10.1016/j.atmosenv.2011.10.015, 2012.
- 819 Rizwan, A. M., Dennis, Y. C. L., and Liu, C. H.: A review on the generation, determination and mitigation of
820 Urban Heat Island, *J Environ Sci-China*, 20, 120-128, Doi 10.1016/S1001-0742(08)60019-4, 2008.
- 821 Ryu, Y. H., Baik, J. J., and Lee, S. H.: Effects of anthropogenic heat on ozone air quality in a megacity, *Atmos*
822 *Environ*, 80, 20-30, 10.1016/j.atmosenv.2013.07.053, 2013.
- 823 Sailor, D. J., and Lu, L.: A top-down methodology for developing diurnal and seasonal anthropogenic heating
824 profiles for urban areas, *Atmos Environ*, 38, 2737-2748, 10.1016/j.atmosenv.2004.01.034, 2004.
- 825 Schell, B., Ackermann, I. J., Hass, H., Binkowski, F. S., and Ebel, A.: Modeling the formation of secondary
826 organic aerosol within a comprehensive air quality model system, *J Geophys Res-Atmos*, 106, 28275-28293, Doi
827 10.1029/2001jd000384, 2001.
- 828 Stockwell, W. R., Middleton, P., Chang, J. S., and Tang, X. Y.: The 2nd Generation Regional Acid Deposition
829 Model Chemical Mechanism for Regional Air-Quality Modeling, *J Geophys Res-Atmos*, 95, 16343-16367, Doi
830 10.1029/Jd095id10p16343, 1990.
- 831 Stone, B.: Urban sprawl and air quality in large US cities, *J Environ Manage*, 86, 688-698,
832 10.1016/j.jenvman.2006.12.034, 2008.



- 833 Wang, X. M., Lin, W. S., Yang, L. M., Deng, R. R., and Lin, H.: A numerical study of influences of urban
834 land-use change on ozone distribution over the Pearl River Delta region, China, *Tellus B*, 59, 633-641,
835 10.1111/j.1600-0889.2007.00271.x, 2007.
- 836 Wang, T., Wei, X. L., Ding, A. J., Poon, C. N., Lam, K. S., Li, Y. S., Chan, L. Y., and Anson, M.: Increasing
837 surface ozone concentrations in the background atmosphere of Southern China, 1994-2007, *Atmos Chem Phys*, 9,
838 6217-6227, 2009.
- 839 Wang, X. M., Chen, F., Wu, Z. Y., Zhang, M. G., Tewari, M., Guenther, A., and Wiedinmyer, C.: Impacts of
840 Weather Conditions Modified by Urban Expansion on Surface Ozone: Comparison between the Pearl River
841 Delta and Yangtze River Delta Regions, *Adv Atmos Sci*, 26, 962-972, 10.1007/s00376-009-8001-2, 2009.
- 842 Wu, J. B., Chow, K. C., Fung, J. C. H., Lau, A. K. H., and Yao, T.: Urban heat island effects of the Pearl River
843 Delta city clusters-their interactions and seasonal variation, *Theor Appl Climatol*, 103, 489-499,
844 10.1007/s00704-010-0323-6, 2011.
- 845 Wu, K., and Yang, X. Q.: Urbanization and heterogeneous surface warming in eastern China, *Chinese Sci Bull*, 58,
846 1363-1373, 10.1007/s11434-012-5627-8, 2013.
- 847 Xie, M., Zhu, K. G., Wang, T. J., Yang, H. M., Zhuang, B. L., Li, S., Li, M. G., Zhu, X. S., and Ouyang, Y.:
848 Application of photochemical indicators to evaluate ozone nonlinear chemistry and pollution control
849 countermeasure in China, *Atmos Environ*, 99, 466-473, 10.1016/j.atmosenv.2014.10.013, 2014.
- 850 Xie, M., Zhu, K. G., Wang, T. J., Feng, W., Zhu, X. S., Chen, F., Ouyang, Y., Liu, Z. J.: Study on the distribution
851 of anthropogenic heat flux over China, *China Environmental Science*, 35, 728-734, 2015.
- 852 Xie, M., Liao, J., Wang, T., Zhu, K., Zhuang, B., Han, Y., Li, M., Li, S.: Modeling of the anthropogenic heat
853 flux and its effect on regional meteorology and air quality over the Yangtze River Delta region, China, *Atmos.*
854 *Chem. Phys.*, 16, 6071-6089, 10.5194/acp-16-6071-2016, 2016.
- 855 Yu, M., Carmichael, G. R., Zhu, T., and Cheng, Y. F.: Sensitivity of predicted pollutant levels to anthropogenic
856 heat emissions in Beijing, *Atmos Environ*, 89, 169-178, 10.1016/j.atmosenv.2014.01.034, 2014.
- 857 Zhang, D. L., Shou, Y. X., and Dickerson, R. R.: Upstream urbanization exacerbates urban heat island effects,
858 *Geophys Res Lett*, 36, Artn L24401
859 10.1029/2009gl041082, 2009.
- 860 Zhang, Q., Streets, D. G., Carmichael, G. R., He, K. B., Huo, H., Kannari, A., Klimont, Z., Park, I. S., Reddy, S.,
861 Fu, J. S., Chen, D., Duan, L., Lei, Y., Wang, L. T., and Yao, Z. L.: Asian emissions in 2006 for the NASA
862 INTEX-B mission, *Atmos Chem Phys*, 9, 5131-5153, 2009.
- 863 Zhang, Y. N., Xiang, Y. R., Chan, L. Y., Chan, C. Y., Sang, X. F., Wang, R., and Fu, H. X.: Procuring the regional
864 urbanization and industrialization effect on ozone pollution in Pearl River Delta of Guangdong, China, *Atmos*
865 *Environ*, 45, 4898-4906, 10.1016/j.atmosenv.2011.06.013, 2011.
- 866 Zheng, J. Y., Zhang, L. J., Che, W. W., Zheng, Z. Y., and Yin, S. S.: A highly resolved temporal and spatial air
867 pollutant emission inventory for the Pearl River Delta region, China and its uncertainty assessment, *Atmos*
868 *Environ*, 43, 5112-5122, 10.1016/j.atmosenv.2009.04.060, 2009.
- 869 Zhu, K., Blum, P., Ferguson, G., Balke, K. D., and Bayer, P.: The geothermal potential of urban heat islands,
870 *Environ Res Lett*, 5, Artn 044002
871 10.1088/1748-9326/5/4/044002, 2010.
- 872 Zhu, B., Kang, H. Q., Zhu, T., Su, J. F., Hou, X. W., and Gao, J. H.: Impact of Shanghai urban land surface forcing
873 on downstream city ozone chemistry, *J Geophys Res-Atmos*, 120, 4340-4351, 10.1002/2014JD022859, 2015.
- 874